Citation
Zhong, Y. and Xu, X. and Liu, Y. and Wang, W. and Shao, Z. 2018. Recent progress in metal–organic frameworks for lithium–sulfur batteries. Polyhedron. 155: pp. 464-484. http://doi.org/10.1016/j.poly.2018.08.067

Review

Recent Progress in Metal–Organic Frameworks for Lithium–Sulfur Batteries

Yijun Zhong[a], Xiaomin Xu[a], Yu Liu[a], Wei Wang[a] and Zongping Shao[a,b,*]

[a] WA School of Mines: Minerals, Energy and Chemical Engineering (WASM-MECE), Curtin University, Perth, WA 6845, Australia.
[b] Jiangsu National Synergetic Innovation Center for Advanced Materials (SICAM), State Key, Laboratory of Materials-Oriented Chemical Engineering, College of Chemical Engineering, Nanjing Tech University, No. 5 Xin Mofan Road, Nanjing 210009, P.R. China.
* E-mail address: zongping.shao@curtin.edu.au (Z. Shao)

Keywords: Lithium–sulfur battery, Metal–organic framework, Coordination polymer, Polysulfide, Lewis acid−base interaction

Abstract

The development of novel electrochemical energy storage systems has induced a great evolution of sustainable production and life. Lithium–sulfur (Li–S) batteries show a significant potential of becoming the next-generation energy storage systems, even though several vital problems, especially the dissolution and loss of active polysulfides, still hinder their practical application. Metal–organic frameworks (MOFs), a novel class of porous crystalline materials, and their derived materials, exhibit great potential for anchoring soluble polysulfides due to the unique physical and surface chemical property. In this review, we dedicate to review strategies for designing MOF-based and MOF-derived materials as hosts and functional polysulfide barriers for Li–S batteries. By revisiting three most important parameters for the design of hosts, namely conductivity, porosity and chemisorption to polysulfides, we hope to gain a greater understanding of how these MOF-related materials promote the electrochemical performance and the cycle stability of Li–S batteries. We also summarize the recent advances of two types of polysulfide barriers working based on an adsorbing-reutilization approach and a blocking approach. Finally, we point out the main challenges and some perspectives for the future development of this promising area.

Graphical Abstract

This review summarizes the recent progress on MOF-based and MOF-derived materials as hosts and as functional polysulfide barriers for Li–S batteries. The review offers greater understanding of this promising research field by revisiting three most important parameters for the design of hosts, namely conductivity, porosity and chemisorption to polysulfides.

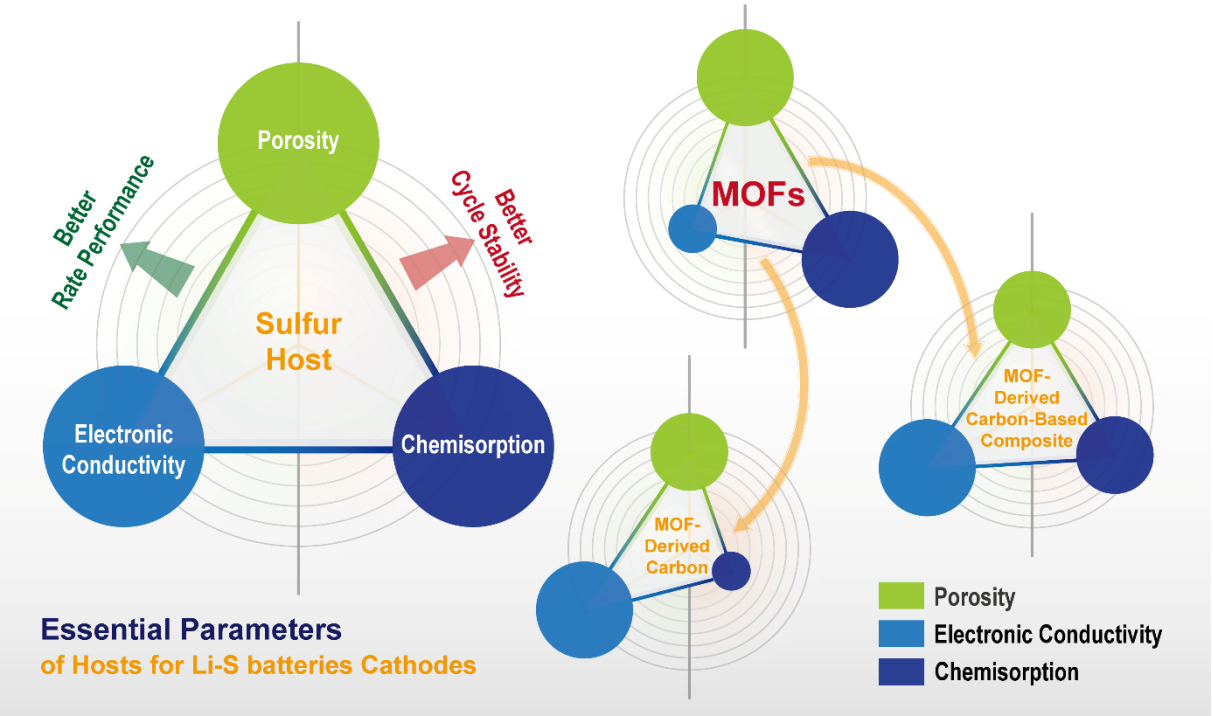

Contents

1. Introduction
2. MOF-based materials as sulfur hosts
   2.1 Interaction with polysulfides
   2.2 Particle size and pore structure modification
   2.3 Electrical conductivity optimization
   2.4 A brief summary
3. MOF-derived materials as sulfur hosts
   3.1 MOF-derived carbons
   3.2 MOF-derived carbon-based composites
   3.3 A brief summary
4. Functional barriers for polysulfides
   4.1 Adsorptive interlayers
   4.2 Blocking separators
   4.3 A brief summary
5. Conclusion and perspectives

Acknowledgements

References

1. Introduction

Conventional applications based on fossil energies would encounter inevitable challenges in the next few decades like limited supply and inevitable environmental pollution. The development of novel electrochemical energy storage systems offers an more efficient and eco-friendly way of sustainable production and life.[1,2] In the past decades, rechargeable lithium-ion (Li-ion) battery has successfully provided solutions for a wide range of electrical applications such as small portable electronic devices, electronic vehicles, unmanned aerial vehicles and large-scale power storage stations.[3–5] However, commercial cathode materials based on an insertion-type reaction suffer from low capacity.[6,7] Intensive research on novel conversion-type cathodes with much higher theoretical capacities has depicted a better future of Li-ion battery.[8,9] Sulfur is one of the most promising candidates of the conversion-type cathode materials due to the high theoretical capacity, vast natural abundance, and low cost.[10] Li−S batteries that apply elemental sulfur as the cathode and lithium metal as the anode can provide a large gravimetric energy density up to 2600 Wh kg^{-1}.[11,12] These advantages of the sulfur cathode and the promising applications of Li−S batteries have stimulated rapid development in this research field.[13]

Figure 1a shows the typical configuration of a Li−S battery, where fundamental reaction mechanism of the S cathode follows a simple overall process of $S_8 + 16Li^+ + 16e^- \leftrightarrow 8Li_2S$.[14] This lithiation/delithiation process takes place via several steps.[15,16] As illustrated in **Figure 1b**, for a typical Li−S battery cathode with elemental sulfur (S_8) molecules as the initial active material, S_8 is first lithiated at higher potential between ~2.3 and ~2.0 V (vs. Li/Li^+) producing high-order lithium polysulfides (Li_2S_n, $4 \leq n \leq 8$).[17] The high-order lithium polysulfides further react with Li-ion producing low-order Li_2S_n ($n \leq 3$) and eventually Li_2S at a lower potential of ~2.0 V.[15] In the reverse process, Li_2S is delithiated stepwise to S_8.

Unfortunately, the practical application of a Li−S battery is currently hindered by several vital drawbacks. First, the electrical conductivity of sulfur is very low (5×10^{-30} S cm^{-1} at 25 °C), resulting in an unacceptable resistance for practical use.[18] Second, for most Li−S batteries with liquid organic electrolyte, the intermediate high-order lithium polysulfides (Li_2S_n, $4 \leq n \leq 8$) are highly soluble.[19–21] The dissolved polysulfides could leave the cathode and result in a deteriorating capacity.[22] In addition, the polysulfides may diffuse and penetrate the separator and react with lithium metal anode, generating irreversible deposits on the anode surface.[23,24] Furthermore, during repeated discharging/charging processes, the polysulfides could shuttle between the cathode and anode, resulting in low Coulombic efficiency.[13] Finally, due to the different densities of S_8 and Li_2S, sulfur undergoes a severe volume

expansion of ~80% during the discharge, which could also lead to failure of the cathode structure.[25,26]

To tackle the issues mentioned above, different types of hosts with distinctive compositions and morphologies have been developed, such as porous amorphous carbons[27–31], graphene[32–34], graphene oxides (GO)[35,36], carbon nanotubes (CNTs)[37–39] and metal compounds (e.g. TiO_2, MnO_2, CoS_2, VN)[40–45]. As illustrated in **Figure 1c**, an ideal host should have sufficient porosity, high electrical conductivity and decent surficial chemisorption capability to polysulfides. Among these three parameters, the porosity of hosts is considered the most important one. Usually, carbon hosts provide excellent electronic conductivity and sufficient porosity. However, limited surficial adsorptive capability to polysulfide can be obtained even by further functionalization with hetero-atoms like oxygen and nitrogen.[46] On the contrary, most of the metal compounds demonstrate decent intrinsic adsorptive feature to polysulfides, but the low porosity (e.g., specific surface area < 400 $m^2 g^{-1}$) of most of the metal compound hosts constrains their advantages due to insufficient volume for high sulfur loading and insufficient surface for effective interactions.[44, 45]

Metal–organic frameworks (MOFs) represent a sort of material with a well-ordered framework composed of metal ions and polyfunctional organic ligands.[47,48] With unique advantages such as high surface area of up to 3000 $m^2 g^{-1}$, high porosity of more than 0.5 $cm^3 g^{-1}$ and adjustable pore size, MOFs have been successfully utilized in many energy applications including Li−S batteries.[49–51] The history of applying MOFs in Li−S batteries can date back to 2011 when Tarascon and co-workers proposed a mesoporous chromium trimesate MOF named MIL-100(Cr) as a host.[52] Since then, exciting progress on the use and optimization of a variety of MOFs (e.g., ZIF-8 [53,54], HKUST-1 [55,56], MIL-101(Cr)[57], and MOF-5 [58]) for Li–S batteries has been achieved. Owing to the low electrical conductivity, the extent of sulfur utilization in these MOFs hosts remains quite low. Intergration MOF hosts with high-conductive carbons or producing MOF-derived carbon-based materials are useful strategies for improving the electrical conductivity. Rationally designed MOF-based and MOF-derived materials demonstrate great balance of porosity, electrical conductivity, and surficial chemisorption. The strategic applications of MOF-related materials as hosts for Li−S batteries are illustrated in **Figure 1d** where advantages and drawbacks of these hosts are also indicated. We will critically discuss these pros and cons in the following sections.

A battery configuration can be also applied for improving the performance of Li−S batteries. As was first proposed by Manthiram and co-workers in 2012, a conceptional functional interlayer was inserted between the cathode and anode to act as a second current collector and

a polysulfide adsorptive barrier.[59,60] In 2016, Zhou and co-workers proposed a novel blocking strategy offering an alternative approach for the confinement of polysulfides.[61] The new polysulfide barrier composed of a dense MOF film shows exclusive sieving effect for small lithium ions and large lithium polysulfides.

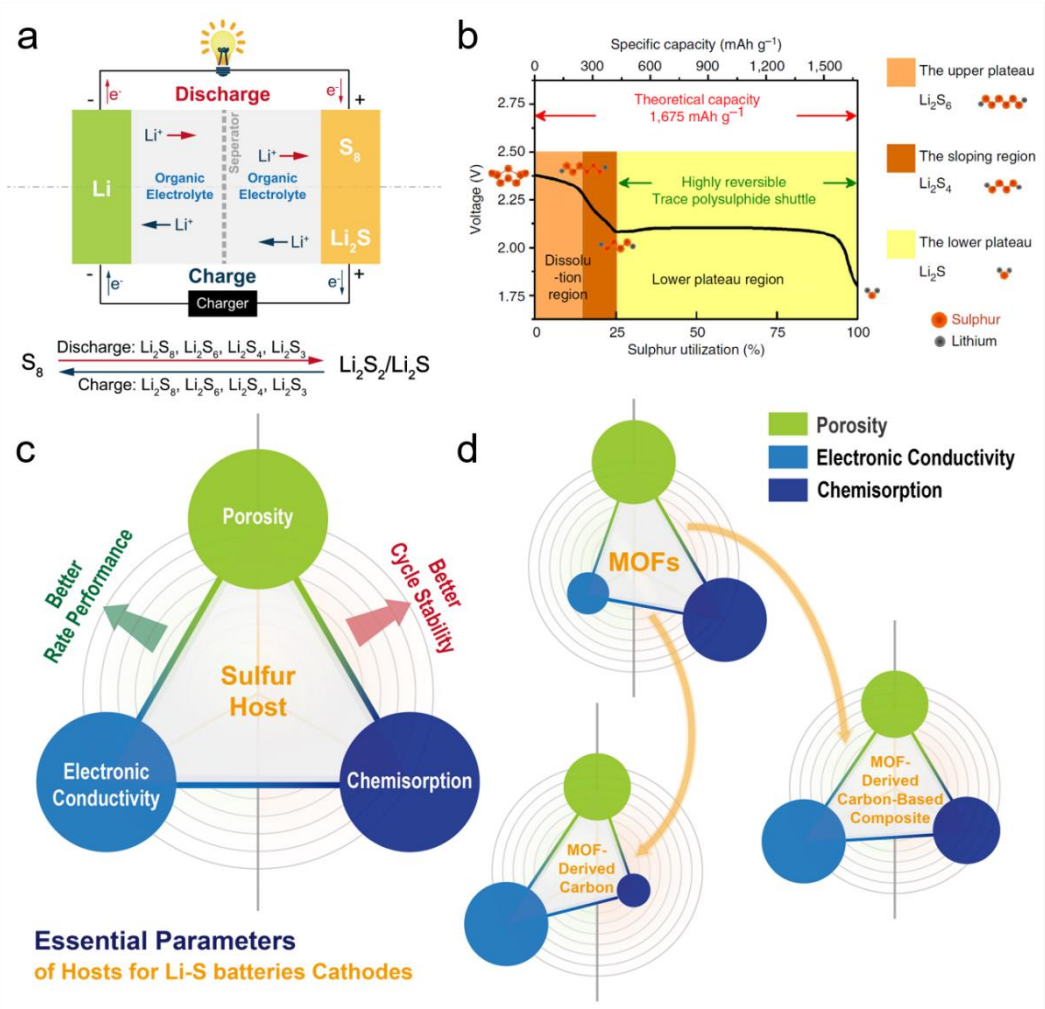

Figure 1 (a) The discharge-charge reaction mechanism of a Li–S battery, (b) The typical discharge profile of Li–S batteries and the sulfur transformations at corresponding potentials, (c) Illustration of the correlation of three essential parameters for advanced sulfur hosts and (d) Advantages and drawbacks of state-of-the-art MOF-based and MOF-derived hosts. Reprinted with permission from (b) [15] Copyright 2013 Springer Nature.

So far, several review articles have mentioned the application of MOF materials for Li–S batteries in a subsection or paragraphs.[2,46,62–66] This review is dedicated to cover the very recent advances and provide more insightful understanding of this topic by indicating the correlation of essential parameters for designing new MOF-related materials for Li–S batteries. In this contribution, we mainly focus on the strategies for designing MOFs and the derived materials for improving performance and stability of Li–S batteries. The physical characteristics and the performance of most MOF-based and MOF-derived hosts are summarized. The challenges and solutions for the MOF-based materials, MOF-derived carbons

and MOF-derived carbon-based composites are demonstrated. The essential parameters and the corresponding modification approaches for state-of-the-art hosts are summarized and discussed. Especially, the unique Lewis acid−base interaction between MOFs and polysulfides is discussed. The catalytic effect on facilitating the redox process of sulfur with MOF-derived transition metal particles is also covered. Finally, we summarize the development of two types of polysulfide barriers which work based on an adsorbing-reutilization approach or a blocking approach. Some perspectives for future development of the MOF-related materials for Li−S batteries are also proposed.

2. MOF-based materials as sulfur hosts

As novel sulfur hosts for Li–S batteries, state-of-the-art MOFs have significant advantages and notorious drawbacks, as illustrated in **Figure 1d**. One of the most unique advantages is the well-defined pore structure with both high pore volume and high specific surface area, which is summarized in **Table 1**. In addition, due to the well dispersed unsaturated metal centers, MOFs have favorable coordination ability to sulfur species (sulfur, lithium polysulfides and lithium sulfide).[67] However, because of the intrinsically low electrical conductivity, S/MOF cathode could suffer from a sluggish charge transfer. In this section, the recent development of various MOF-based hosts is summarized. The interaction between MOFs and sulfur will be first discussed, followed by the discussion upon the tuning strategies on particle sizes, pore structure and conductivity of the MOF-based materials.

2.1. Interaction with polysulfides

A groundbreaking work where MOF was first used as the host for Li–S battery cathode was published by Tarascon and co-workers.[52] They reported the synthesis of MIL-100(Cr) featuring a unique well-defined hierarchical pore structure with 25–29 Å mesoporous cages connected by 5 Å and 9 Å microporous windows. The structure provides a high pore volume of 0.95 $cm^3\ g^{-1}$ for sulfur accommodation and a high specific surface area of 1485 $m^2\ g^{-1}$ for effective surface interaction to polysulfides. After 48 wt% sulfur loading using a facile melt diffusion method, the as-obtained cathode demonstrated a decent sulfur utility and cycling stability at that time. Considering the intrinsically low electrical conductivity of the MOF, a high amount (50 wt%) of conductive carbon additive was added into the cathode. While the initial discharge capacity of the cathode with the MOF host (~1100 mA h g^{-1} at 0.1 C) was lower than those of the mesoporous carbon hosts, the cathode with the MOF host presented a much better cycle stability (**Figure 2a**). Further analysis of the XPS S 2p spectra of sulfur (**Figure 2b**) and the MOF sample after sulfur infiltration (**Figure 2c**) indicated a complex

interaction between sulfur and the inorganic moieties, which could provide additional polysulfides trapping function and thus contribute to the improved cycle stability. This work stimulated a series of research which utilized a wide range of MOF and MOF-based materials as the host for Li–S batteries.[55,57,68–73]

Table 1 Physical parameters and performances of MOF-based hosts for Li–S batteries.

MOF	Functional Additive	Specific Surface Area	Total Pore Volume	Sulfur in Composite	Areal Sulfur Loading	Conductive Carbon in Cathode	Initial Discharge Capacity	Cycling Capacity	High-rate Performing Capacity	Ref.
		$m^2\ g^{-1}$	$cm^3\ g^{-1}$	%	mg cm g^{-2}	%	mAh g^{-1}	mAh g^{-1}	mAh g^{-1}	
MIL-100(Cr)	(None)	1485	0.95	48	/	50	~1100, 0.1 C	450, 60th, 0.1 C	/	[52]
MIL-100(V)	rGO*[1]	1582 (MOF)	0.21 (MOF-rGO)	50	0.9−1.0	20	~1000, 0.05 C	500, 200th, 0.5 C 450, 300th, 0.5 C	570, 0.5 C	[74]
MIL-101(Cr)	rGO	1022 (MOF-rGO)	0.38 (MOF-rGO)	50	1.5	10	980, 0.2 C	650, 50th, 0.2 C	/	[69]
MIL-101(Cr)	Graphene	3483 (MOF)	1.5 (MOF)	59	/	20	1193, 0.1 C	847, 134th, 0.8 C	500, 3.0 C	[57]
MIL-101(Cr)	PEDOT:PSS*[2]	3412 (MOF)	/	56	0.9	10	1568, 0.1 C	607, 192th, 0.1 C	158, 1 C	[75]
MIL-101(Cr)	ppy*[3]	3250	/	37	0.8−1.4	20	~950, 0.3 C	320, 400th, 5 C	320, 5 C	[76]
MIL-53(Al)	(None)	/	0.54	50	/	30	1215, 0.1 C	347, 300th, 0.5 C	~350, 1 C	[53]
NH_2-MIL-53(Al)	(None)	/	0.57	50	/	30	1125, 0.1 C	332, 300th, 0.5 C	~500, 1 C	[53]
MIL-53(Al)	ppy	1370 (MOF)	/	37−60	0.8−1.4	20	1420, 0.1 C	900, 100th, 0.5 C 480, 400th, 5 C (S: 41%)	480, 5 C (S: 41%)	[76]
HKUST-1 (CuBTC)	(None)	1500	/	40	0.5	35	1498, 0.05 C	~500, 170th, Discharge 0.05 C Charge 0.1 C	/	[55]
HKUST-1 (CuBTC)	(None)	~140	0.16	32	/	0	~350, 0.2 C (based on cathode)	~250, 1000th, 0.2 C (based on cathode)	~200, 1 A g^{-1} (based on cathode)	[71]
HKUST-1 (CuBTC)	CNTs	/	/	40−70	1−11	0	1263, 0.2 C (S: 40%, 1 mg cm^{-2})	851, 200th, 0.2 C 681, 500th, 0.2 C (S: 40%, 1 mg cm^{-2})	449, 10 C (S: 40%, 1 mg cm^{-2})	[56]
HKUST-1 (CuBTC)	(None)	/	/	65	/	15	679, 0.1 C	~330, 100th, 0.2 C	/	[77]
ZIF-8	(None)	/	/	30	/	35	~1350, 0.05 C	420, 200th, 0.1 C	450, 1 C	[68]

ZIF-8	MWCNTs*[4]	1066 (MOF-CNT)	0.51 (MOF-CNT)	/	~0.5	15	~1600, 0.05 C	380, 25th, 0.1 C	/	[70]
ZIF-8	(None)	/	0.70	50	/	30	1055, 0.1 C	553, 300th, 0.5 C	710, 1 C	[53]
ZIF-8	(None)	1672	0.64	54	1.0	30	~1300, 0.5 C	~600, 250th, 0.5 C	/	[54]
ZIF-8	CNT Sponge	1136 (MOF-CNT)	0.88 (MOF-CNT)	64	8	/	1380, 0.1 C	1269, 100th, 0.1C 750, 500th, 1 C	840, 1 C	[78]
Tannic Acid Tuned ZIF-67	(None)	369	/	67	/	15	~1500, 1 A g^{-1}	757, 100th, 0.1 A g^{-1} 521, 550th, 0.5 A g^{-1}	510, 1.6 A g^{-1}	[73]
MOF-5	(None)	684	0.42	50	1.9	20	1476, 0.2 C	609, 200th, 0.2 C	/	[58]
$Ni_6(BTB)_4(BP)_3$	(None)	5243	2.15	60	/	10	689, 0.1 C	~550, 200th, 0.1 C	287, 2 C	[79]
Co_6 $(BTB)_4(BP)_3$	(None)	/	/	/	/	10	~580, 0.2 C	~400, 200th, 0.2 C	/	[79]
MOF-525(2H)	(None)	/	/	50	0.7	20	~1200, 0.5 C	402, 200th, 0.5 C	~250, 5 C	[80]
MOF-525(FeCl)	(None)	/	/	50	0.7	20	~1150, 0.5 C	616, 200th, 0.5 C	~350, 5 C	[80]
MOF-525(Cu)	(None)	/	/	50	0.7	20	~1180, 0.5 C	704, 200th, 0.5 C	~400, 5 C	[80]
$[(CH_3)_2NH_2]_2$[Cd (L)] ·5DMF	(None)	/	/	72	1.0	20	1092, 0.1 C	799, 50th, 0.1 C	571, 1 C	[81]
nMOF-867	(None)	2250	/	50	/	/	1121, 0.1 C	~700, 500th, 0.5 C	/	[82]
nUiO-67	(None)	2256	/	50	/	/	1115, 0.1 C	~450, 500th, 0.5 C	/	[82]
UiO-66	CNT	1157	0.43	68	~1	10	925, 0.5 A g^{-1}	765, 300th, 0.5 A g^{-1}	411, 2A g^{-1}	[83]
Prussian Blue Analogues	PEDOT	518 (MOF)	0.72	55-82	1.1	10	1291, 0.1 C	544, 200th, 5 C	683, 5 C	[84]
Cu-TDPAT	(None)	1473	0.55	50	1.2	10	~1100, 0.1 C	831, 300th, 0.5 C 745, 500th, 1 C	523, 5 C	[85]
PCN-224	ppy	2660 (MOF)	/	55	0.8−1.4	20	1330, 0.5 C	820, 200th, 5 C 670, 200th, 10 C 440, 1000th, 10 C	820 5 C 670, 10 C	[76]

NOTE:
*[1] rGO: reduced graphene oxide
*[2] PEDOT: conductive polymer poly(3,4-ethylenedioxythiophene). PSS: Poly(3,4-ethylenedioxythiophene)/poly(styrene sulfonate)
*[3] MNCNTs: multi-wall carbon nanotube
*[3] ppy: polypyrrole

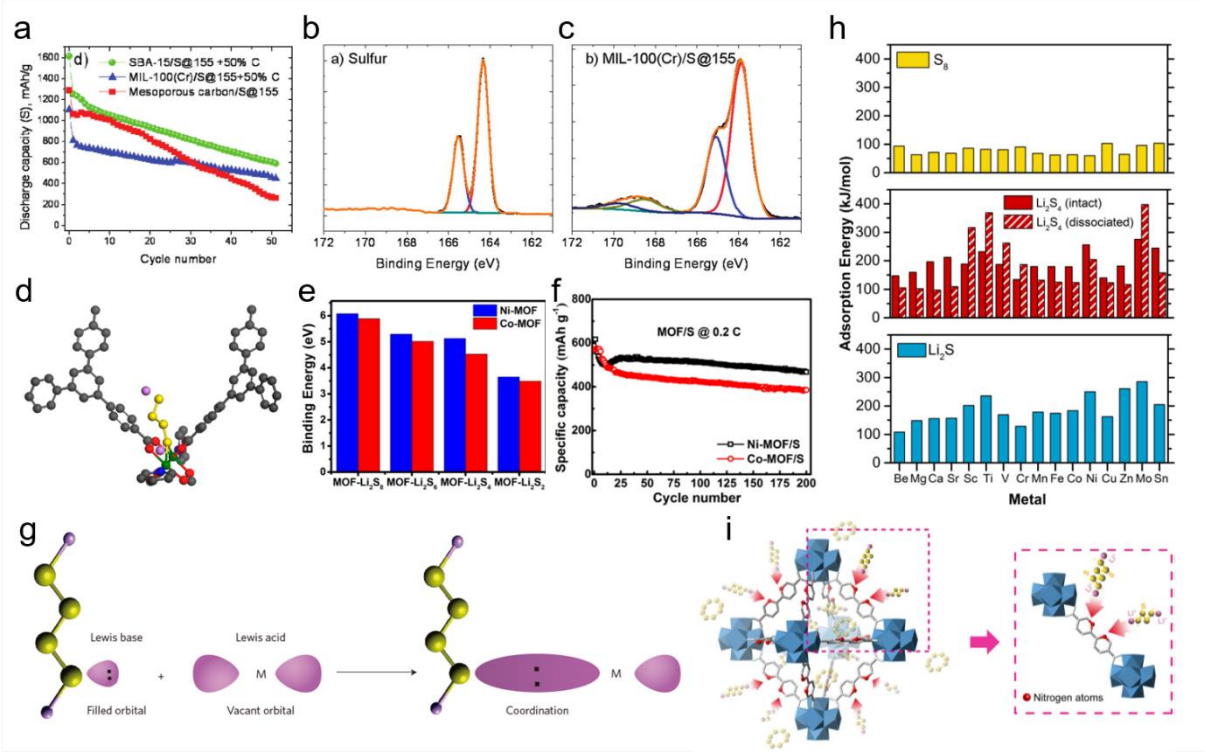

Figure 2 (a) Cycling performance of cathodes with MIL-100(Cr) host, mesoporous carbon host and SBA-15 host at 0.1 C, (b) XPS S 2p spectrum of elemental sulfur, (c) XPS S 2p spectrum of MIL-100(Cr)/S, (d) Illustration of the binding between polysulfides and Ni-MOF, (e) Binding energies of polysulfides to Ni-MOF and Co-MOF, (f) Cycling performance of cathodes with Ni-MOF host and Co-MOF host at 0.2 C, (g) Illustration of the interaction between the polysulfide Lewis base and the transition metal acid center, (h) Adsorption energies for S_8, Li_2S_4, and Li_2S within the M_2(dobdc) MOF (M = different metal), and (i) Illustration of the interaction between nitrogen atoms in nMOF-867 and lithium polysulfides. Reprinted with permission from (a)–(c) [52] Copyright 2011 American Chemical Society, (d)–(f) [79] Copyright 2014 American Chemical Society, (g) [46] Copyright 2016 Springer Nature, (h) [86] Copyright 2017 American Chemical Society, (i) [82] Copyright 2016 Springer Nature.

2.1.1. Lewis acid−base interaction

However, the chemical interaction between MOFs and sulfur species was not well understood until a Lewis acid−base theory was introduced by Xiao and co-workers [79] In their work, Ni-MOF was studied as a sulfur host which provides both physical and chemical interaction for anchoring polysulfides. Ni/MOF/S composite with a sulfur content of 60 wt% demonstrated an excellent cycling performance. Besides the physical confinement of polysulfides with the bimodal porous matrix, strong Lewis acid−base interaction further slows down the migration of dissolved polysulfides (**Figure 2d**). In the interaction, the exposed coordinated Ni(II) node in the MOF serves as a soft Lewis acidic site, while the dissolved polysulfide anion acts as a soft Lewis basic site (**Figure 2g**). Binding energies between Ni-MOF and polysulfides with different chain lengths were evaluated using a first principle calculation based on the density functional theory (DFT) (**Figure 2e**). The high binding energy of up to ~6 eV is superior to those of the typical chemisorption reagents like heteroatom-doped carbons (1.3–2.6 eV), and stoichiometric metal chalcogenides (2.6–3.5 eV).[46] Inspired by

Xiao's work, the Lewis acid−base theory has been widely applied to explain the effective sulfur anchoring of MOF-based hosts in many publications.[58,80,85]

2.1.2. Influence of Metal Nodes

Actually, a wide range of metal nodes (e.g., Mg, Cu, Mn, Ni, Co, Zr, Fe, Zn) can serve as the acidic site for Lewis acid–base interaction.[67] Therefore, investigation into their influence on the sulfur anchoring is very important. By comparing the binding energies to polysulfides and the battery stabilities (**Figure 2e&f**), Xiao and co-workers found that the interaction of Ni node to polysulfides is more stable than that of Co node in a $M_6(BTB)_4(BP)_3$ (M = metal) matrix.[79] This result is consistent with the Irving-Williams Series, which shows that the stabilities of a metal complex follow the order of Mn < Fe < Co < Ni < Cu (all having a +2 oxidation state).[87] Park and Siegel used a computational method to screen 16 different substituted metals based on a M_2(dobdc) matrix (MOF-74).[86] As illustrated in **Figure 2h**, the adsorption energies for different metal nodes with S_8, Li_2S_4, and Li_2S in the MOF-74 matrix are compared. The result shows that Ti, Ni, and Mo have largest affinities for Li_2S_4 and Li_2S. The number of active sites on a MOF unit can be tuned by varying the local environments at the center of the porphyrin moieties. For example, Wang et al. prepared a series of MOF-525(Cu) with H^+, Fe^{3+}-Cl, and Cu^{2+} as the Lewis active sites that respectively provide 0, 1 and 2 sites for the Lewis acid–base interaction.[80] The MOF-525(Cu) host showed better sulfur confinement with a capacity of ~700 mAh g^{-1} after 200 cycles at 0.5 C.

2.1.3. Influence of organic ligands

Several works have reported that the modification of organic ligands may also have an influence on the polysulfides anchoring. Park et al. prepared two MOFs with and without sp^2 N atoms in the organic ligands.[82] In situ spectroelectrochemical results indicate that the nMOF-867 with sp^2 N atoms have better capability for sulfur confining, thus demonstrating better stability of the batteries (**Figure 2i**). A bifunction Cu-TDPAT with both Lewis acidic sites and Lewis basic sites to synergistically establish strong interaction to polysulfides was proposed by Hong et al.[85] The exposed Cu(II) nodes served as Lewis acidic sites binding with sulfur atoms in polysulfides. At the same time, the N atoms in the organic ligands served as Lewis basic sites binding with lithium ions. This synergistic binding gave rise to an effective sulfur anchoring, endowing excellent cycling performance of the batteries. However, introducing groups on organic ligands may also have a negative effect. In another work reported by Zhou et al., the battery performance of the NH_2-MIL-53 host with Lewis basic group (−NH_2) was inferior to

that of the MIL-53 host.[53] The authors suggested that the Lewis basic amino groups in the organic ligands are unfavorable for the generation and stabilization of polysulfides. This could result in worse charge transfer as well as dampened ion diffusion. Very recently, a UiO-66 with linker-missing defects was reported by Pu et al.[83] First principles calculations indicate that the suitable content of defects may promote the kinetics of chemisorption for polysulfide (Li_2S_6). The result above indicates the complex influence of the organic ligands. Therefore, further design on the modification of ligands is highly demanded, with special attention given to its complexity.

2.2. Particle size and pore structure modification

2.2.1. Particle size modification

Usually, downsizing of the active materials can result in an improved battery performance due to the better ionic accessibility in most Li-ion battery systems. However, owing to the complication of pore structure and the relatively low electrical conductivity in the MOF, more parameters should be taken into consideration for a Li–S cathode with MOF-based hosts. The influence of particle sizes of the MOF hosts was discussed in detail by Zhou et al.[53] ZIF-8 hosts with particle sizes of 150 nm, 1 μm and 3 μm were prepared for comparison. Their result showed a similar cycle stability within 100 cycles at 0.5 C. As presented in **Figure 3a**, the major differences for the cathodes are their maximum capacities and reversible capacities. The MOF host with a smaller particle size demonstrated a higher maximum capacity, indicating better sulfur utilization. This can be ascribed to the shorter ionic diffusion length for the downsized host. However, a higher potential hysteresis was observed for the host with a smaller size, indicating an inferior charge-transfer process compared to the larger hosts. The author ascribed this to the decreased contact point to the same amount of conductive additives. Baumann et al. compared CuBTC (also known as HKUST-1) hosts with particle sizes of 160 nm, 1.6 μm and 5.9 μm, and also concluded that a smaller particle with more external surface could facilitate the ionic diffusion and thus lead to better sulfur utility.[77] A similar observation for Cu-TDPAT hosts with particle sizes ranging from 100–1000 nm was also reported by Hong et al.[85]

In another work, Zhou et al. revisited the influence of particle size and provided more insight into this topic.[54] By comparing ZIF-8 with different particle sizes from 15 nm to 2 μm, they reported that the sulfur utilization increases with the downsizing of the MOF host similar to their previous conclusion. However, the best cycle stability was observed with a moderate size of 200 nm. The 200-nm ZIF-8 host performed as a combination of decent maximum capacity

as well as excellent cycle stability. The author proposed that the surficial sulfur was first lithiated, generating soluble polysulfide. The dissolved polysulfide would either diffuse to the core and further react chemically with the sulfur or escape from the ZIF-8 particle. The two different routes took place at the same time. A host with a too large particle size would lead to internal diffusion pathway becoming too long, thus decreasing the sulfur utility. On the contrary, a host with a too small particle size could result in rapid lithiation of sulfur at the expense of easy polysulfide escaping. Therefore an "golden size" of particle could be carefully optimized.

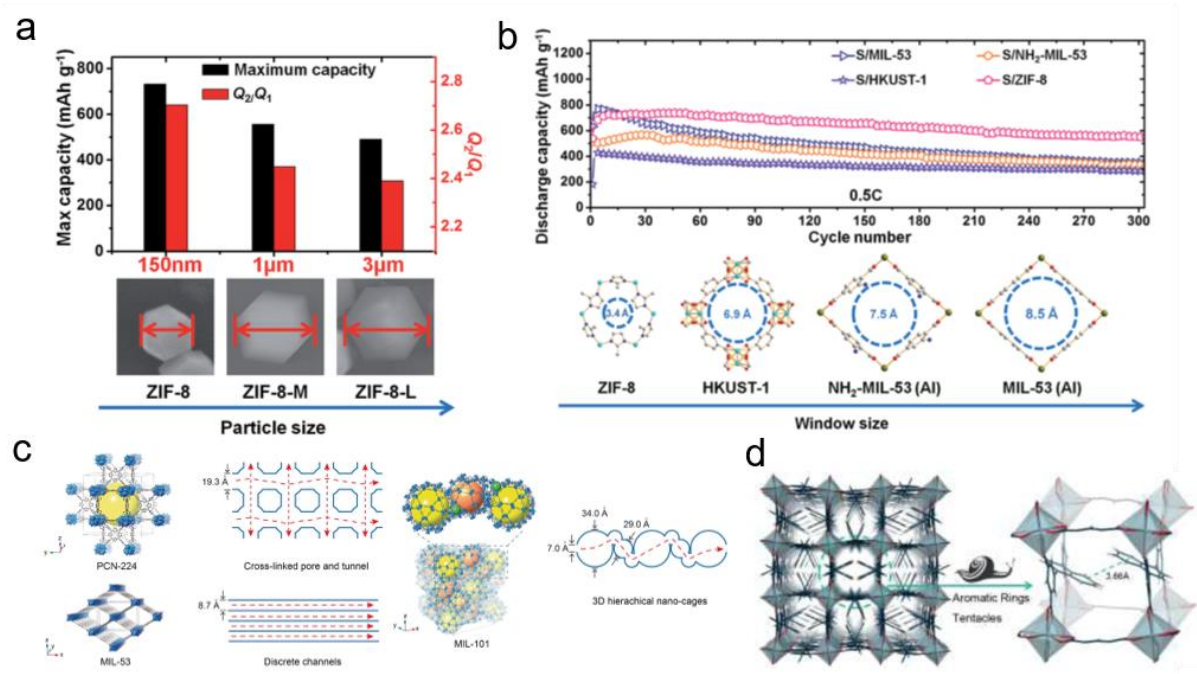

Figure 3 (a) Discharge capacities of cathode with different ZIF-8 host particle sizes, (b) Long-term discharge capacities of cathode with different MOF hosts and the corresponding illustration of the largest window size of the MOF hosts, (c) Illustrations of the crystal structures and the corresponding ion diffusion pathways of PCN-224, MIL-53 and MIL-101, (d) Illustration of the semi-open channels of a MOF host with aromatic rings tentacles. Reprinted with permission from (a), (b) [53] Copyright 2014 Royal Society of Chemistry, (c) [76] Copyright 2018 WILEY-VCH Verlag GmbH & Co. KGaA, Weinheim, and (d) [81] Copyright 2016 American Chemical Society.

2.2.2. Pores modification

The well-defined pore structure with specific pore size, channel (window) diameter as well as pore linkage pathways could be distinctive for each MOF. Sulfur utility and confinement in Li–S batteries with MOF-based hosts could also be affected by these structural parameters. The first report on utilizing MOF as the sulfur host highlighted that large pores with small windows are more advantageous to higher sulfur accommodation and better polysulfide confinement.[52] Zhou et al. compared four different MOF (ZIF-8, HKUST-1, NH_2-MIL-53(Al) and MIL-53(Al)) with different pore window sizes.[53] They found that the average capacity fading rates are highly associated with the window sizes (**Figure 3b**). The ZIF-8 host with the smallest window size of 3.4 Å exhibited the best cycle stability.

A different result was presented by Mao et al.[56] They proposed that larger sizes of pore window could facilitate the sulfur infiltration process, therefore improving the cycle stability of the cathode. In their comparison of cathodes with ZIF-8, MOF-5 and HKUST-1, the ZIF-8 host, despite having a smallest window size, demonstrated worse performance relative to the other two hosts. Considering the much smaller window size of ZIF-8 (3.4 Å) compared to the S_8 ring (6.8 Å), the authors indicated that it is difficult for ZIF-8 to accommodate the sulfur using a thermal infiltration method. Most of the sulfur were deposited on the surface of the particle, which resulted in the worse sulfur confinement during cycling.

The impact of pore geometry was investigated by Jiang et al.[76] As illustrated in **Figure 3c**, PCN-224 with cross-linked pores can shorten the ion diffusion pathways. In addition, a large pore window can also facilitate the ion diffusion. Therefore, excellent high-rate (5 C) performance was demonstrated. The authors concluded that a pore geometry with short ion diffusion pathways and with large pore windows are beneficial to the battery performance, especially under high current rates. Li reported a novel MOF with both open channel and semiopen channel (**Figure 3d**).[81] The authors indicated that the open channels could provide higher sulfur loading while the unique semiopen channels with aromatic rings tentacles could offer good sulfur anchoring. The π–π^* conjugated matrix from these channel systems can further facilitate charge transfer and sulfur confinement.

2.3. Electrical conductivity optimization

Until now, most of the MOFs that have been utilized as hosts for sulfur possess similar low electrical conductivity. As listed in **Table 1**, some cathodes with MOF-based hosts in early-stage publications contain a very high content of conductive carbon additives up to 50 wt%.[52,55,68] In addition, even though most of the MOFs have very high pore volume for sulfur accommodation, the sulfur content of the cathodes in many publications are still not comparable to most of the other advanced Li–S battery cathode composites. Furthermore, the relatively low sulfur utilization observed in some of the MOF hosts is also associated with their low conductivity. Approaches to improving the overall electrical conductivity of cathode have been developed by extrinsically composting MOFs with conductive carbons and polymers.

Bao et al. proposed a facile method to embed MIL-101(Cr) into a rGO matrix.[69] By mixing MIL-101(Cr) and GO, a MIL-101(Cr)@rGO was obtained by facilely reducing GO with hydrazine hydrate. The composite showed an improved electrochemical performance. Hou et al. also proposed an in situ synthesis process to produce MIL-100(V) in rGO.[74] Yue et al. proposed a MWCNT@ZIF-8 host which was prepared via a nanotube-facilitated synthesis

using ZnO nanoparticle as the precursor of ZIF-8.[70] This method produced well dispersed ZIF-crystal on the MWCNTs.

In 2017, breathtaking performances obtained from foldable interpenetrated MOF/CNTs thin film hosts were reported by Mao et al.[56] By converting well interpenetrated metal hydroxide nanostrands precursor and CNTs, the resultant MOFs-CNTs network attached in molecular scale allowed a smooth electron transfer throughout the entire electrode (**Figure 4a**). Much improved rate performance was therefore achieved. An excellent reversible discharge capacity of 449 mAh g^{-1} were demonstrated at a very high current density of 10 C for a cathode with the HKUST-1/CNT host. More impressively, the interpenetrated CNTs could also weave the electrode into a foldable cloth, making the electrode possible to work under a 90° bended and even 180° folded situation (**Figure 4b**) The pliable cloth can also buffer the severe volume variation of sulfur during cycling. Very recently, an in-situ growth of ZIF-8 in CNT sponge network was developed by Zhang et al.[78] The mutually embedded ZIF-8 and CNT constructed a highly porous and electrical conductive host structure with high areal sulfur loading of 8 mg cm^{-2}. Remarkable areal capacity of ~11 mAh cm^{-2} and excellent cycling performance were demonstrated.

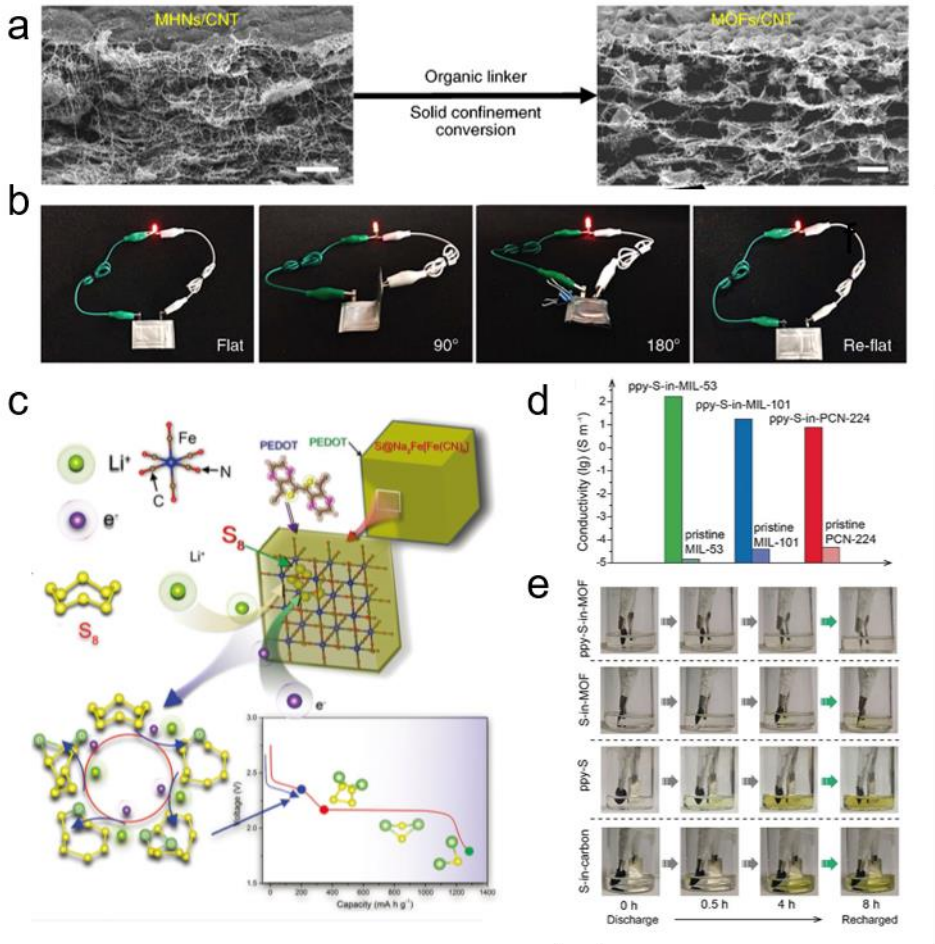

Figure 4 (a) Synthesis of MOFs/CNT composite thin films, left image shows the interpenetrated metal hydroxide nanostrands precursor and CNTs, right image shows the resultant MOFs/CNT product, (b) Digital photos of soft package battery working under flat situation and under bending at 90°, 180°, (c) Illustration of the PEDOT coating on the Prussian blue analogues and the discharge process of the S@ $Na_2Fe[Fe(CN)_6]$@PEDOT cathode, (d) Electrical conductivity of MOF and ppy-S-in-MOF composites, (e) Digital photos of transparent cells with ppy-MOF, MOF, ppy, and porous carbon as hosts in the first discharge-charge. Reprinted with permission from (a), (b) [56] Copyright 2017 Springer Nature, (c) [84] Copyright 2017 WILEY-VCH Verlag GmbH & Co. KGaA, Weinheim, and (d), (e) [76] Copyright 2018 WILEY-VCH Verlag GmbH & Co. KGaA, Weinheim.

Besides the conductive carbon materials, functional conductive polymer coating can also provide a decent improvement of the overall electrical conductivity. Wang and co-authors proposed PEDOT rapped Prussian blue analogues as a novel host for Li–S cathode (**Figure 4c**).[84] The conducive polymer offered better electron accessibility and improved charge transfer. In addition, the PEDOT coating also contributed to additional chemical binding to polysulfides. A similar strategy was proposed by Jin et al., who coated doped-PEDOT:PSS on MIL-101 to improve conductivity.[75] Very recently, a rational design of ppy-S-in-PCN-224 cathode with excellent electron transfer, Li-ion diffusion and polysulfides confinement was developed by Jiang et al.[76] As mentioned in Section 2.2.2, the PCN-224 with cross-linked tunnels is beneficial to the ion diffusion. The polypyrrole (ppy) coating of PCN-224 dramatically increased the electrical conductivity by 5−7 magnitudes (**Figure 4d**). A visible color comparison (**Figure 4e**) of the first discharge-charge process for cathodes with different hosts also indicates the best confinement of polysulfides achieved in the ppy-MOF complex. The combination of excellent electron transfer, Li-ion diffusion and polysulfides confinement ensures an excellent high-rate performance and stability. As a result, an impressive retention capacity of 440 mAh g^{-1} after 1000 cycles was recorded at a high current density of 10 C.

It is worth noting that the development of MOFs with high intrinsic electrical conductivity for Li–S batteries is highly expected. Several pioneering works have reported some unique MOFs with high conductivity.[88] Very recently, a representative MOF (Cu-BHT, with conductivity up to ~1580 S cm^{-1}) has been evaluated by a computational method, which demonstrated its promise as a host for high-performance Li–S batteries.[89] However, no experimental result has been proposed so far.

2.4. A brief summary

MOF-based sulfur hosts show promising long-cycling stabilities in Li–S batteries. Explanation of sulfur confinement based on the Lewis acid–base theory deepens the understanding of interaction between active sulfur species and MOFs. Such chemical interaction between the acidic unsaturated metal nodes and the basic polysulfides can promote

the cycle stability of the batteries. The binding energy of polysulfides with different metal nodes is found to be significantly different. Modifications of the organic ligands could also promote the electrochemical performance. Moreover, the development of well controlled particle sizes and well-designed porous structures with large pore diameter and suitable pore window size can facilitate the sulfur utility, sulfur redox kinetics and long cycle stabilities on a MOF-based hosts. However, the intrinsic insulating character of most MOFs weakens their unique advantages. Approaches to improving the overall electrical conductivity of cathode have been developed, for example, by extrinsically composting MOFs with conductive carbons or functional polymers.

3. MOF-derived materials as sulfur hosts

As demonstrated in the previous section, even though the highly porous MOF materials can accommodate a large amount of sulfur, the full utility of sulfur is still a challenging issue owing to the low electrical conductivity and the complexity of sulfur-MOF interaction. Calcination of MOFs, which produces MOF-derived carbon, carbon-metal composite and carbon-metal compound composites.[90–92] The utilization of MOF-derived materials is an alternative strategy for improving electrical conductivity and simplifying the chemical interaction of the cathode system.

As we illustrated in **Figure 1d**, due to the conductive carbon base, these MOF-derived hosts would no more suffer from low electrical conductivity. These MOF-derived materials inherit the morphological features and highly porous characteristics of the MOF precursors. In this case, the capability of sulfur storage, utility and confinement are strongly associated with the pore volumes of hosts. The pore volumes of hosts not only provide a sulfur storage space but also offer buffer space for the volume variation of sulfur (~80%) during the discharge/charge process ($S_8 + 16Li \rightarrow 8Li_2S$). Base on this consideration, a facile evaluation for the maximum S loading on a host with certain specific total pore volume was proposed in our previous work[93]:

$$x \leq \frac{V_g}{V_g + 0.8631} \quad (1)$$

Where x is the mass loading of sulfur (ranging from 0 to 1) in a sulfur/host composite, and V_g is the total pore volume of the host ($cm^3\ g^{-1}$). The equation can be transformed into:

$$\frac{1}{x} \geq 1 + 0.8631\frac{1}{V_g} \quad (2)$$

Where a linear relation exists between 1/x (ranging from 1 to +∞) and $1/V_g$ (ranging from 0 to +∞), as illustrated by the solid green line in **Figure 5**. The solid green line indicates a maximum sulfur loading where sulfur is trapped only based on the physical capillary sorption provided by

pores of hosts, with sulfur expansion during cycling considered. The area above the solid green line suggests that residual pore is left, while the area below indicates that sulfur cannot be effectively trapped only based on physical sorption. This reveals that both physisorption and chemisorption are essential for most of the MOF-derived hosts. Also, as presented in **Figure 5**, data points (data from **Table 2**) for MOF-derived carbon hosts disperse closer to the green line, indicating higher proportion of physisorption for polysulfide anchoring than chemisorption. For MOF-derived carbon-metal and carbon-metal compound composites, data points (data from **Table 3&4**) sit far away from the green line. This indicates that stronger chemical binding of sulfur species would be provided by the decorated metal/metal compounds.

In this section, the development of a wide range of MOF-derived carbon and carbon-based composites as sulfur hosts for Li–S batteries is reviewed. The dual confinement effect of both physisorption from capillarity and chemisorption from heteroatom-doping and metal incorporation is discussed. The catalytic effect with the transition metal particles for facilitating redox process of sulfur is also included.

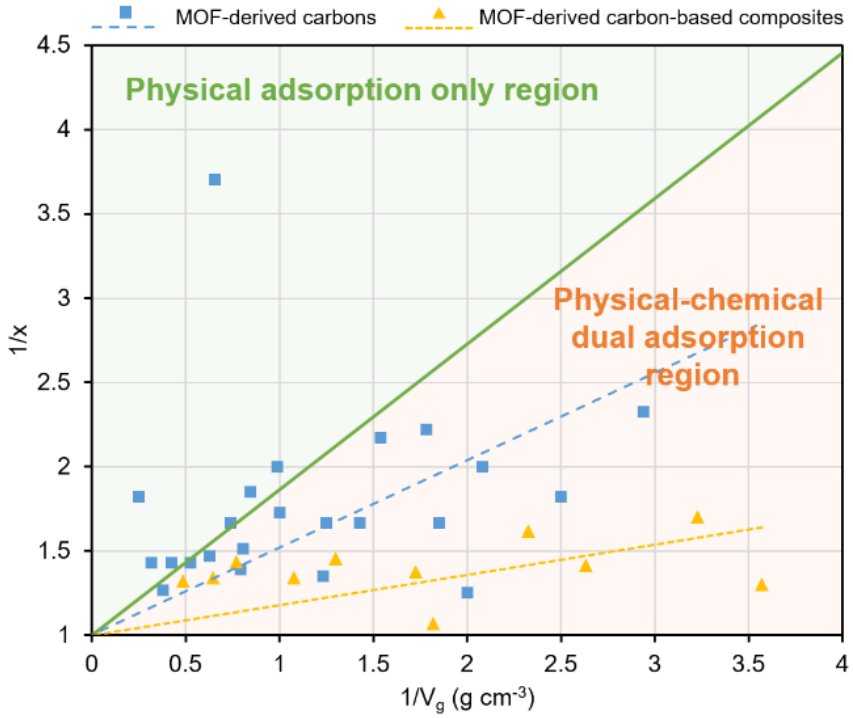

Figure 5 Factor analysis of polysulfide confinement with MOF-derived carbons and MOF-derived carbon-based composites. Data are obtained from the reported total pore volume (V_g) and sulfur content (x, from 0 to 1, based on sulfur and host composite) as listed in **Table 2–4**.

Table 2 Physical parameters and performances of MOF-derived carbons as hosts for Li–S batteries.

MOF Precursor	MOF-Derived Materials	Specific Surface Area	Total Pore Volume	Sulfur in Composite	Areal Sulfur Loading	Initial Discharge Capacity	Cycling Capacity	High-Rate Capacity	Ref.
		$m^2\ g^{-1}$	$cm^3\ g^{-1}$	%	$mg\ cm^{-2}$	$mAh\ g^{-1}$	$mAh\ g^{-1}$	$mAh\ g^{-1}$	
ZIF-8	Micro-C Polyhedrons	849	0.34	43	/	~1500, 100 mA g^{-1}	420, 100th, 100 mA g^{-1}	~250, 1000 mA g^{-1}	[90]
ZIF-8	Graphene Wrapped Micro-C	969	0.40	55	/	1171, 0.1 C	561, 120th, 0.1 C	/	[94]
ZIF-8	N-Doped Micro-C	1105	1.53	27	1	1659, 335 mA g^{-1}	937, 100th, 335 mA g^{-1}	646, 5 A g^{-1}	[95]
ZIF-8	2D Carbon Nanosheets	1228	0.80	60	0.6−0.8	~1200, 0.5 C	~950, 100th, 0.5 C	~600, 1 C	[96]
ZIF-8	Tunable Porous Carbon	1900	~0.7	60−65	0.8	~1500, 0.1 C	~800, 100th, 0.1 C	/	[97]
ZIF-8	N-doped 2D Carbon Nanosheets	3052	2.35	70	2	1226, 0.2 C	~587, 300th, 0.5C	785, 2 C	[98]
ZIF-8	rGO and Meso-C	756	1.24	66	1.5−2.5	1309, 0.2 C	736, 500th, 1 C	683, 2 C	[99]
ZIF-8	3D Nitrogen-Rich Carbon Photonic Crystal Architecture	2546	13.42 (Mecury Intrusion)	78	2	1160, 0.2 C	534, 1000th, 0.5 C	967, 2 C	[100]
ZIF-8	3D rGO@ N-doped Porous Carbon Polyhedron/CNTs	850	1.59	68	1.2−1.4	~1150, 0.2 C	660, 200th, 0.2 C	/	[101]
ZIF-8	N-Doped Carbon	1032	0.54	55−60	0.8−3.0	~1150, 300 mA g^{-1} (S: 60%)	529, 180th, 300 mA g^{-1} (S: 60%)	~400, 1600 mA g^{-1} (S: 60%)	[102]
ZIF-8	3D N-doped CNTs- Carbon Nanosheets – Porous Carbon	856	/	70	1.5–2.5	1442, 0.1 C	564, 700th, 1 C	618, 2 C	[103]
ZIF-8	N-doped hierarchically Porous Multilayered Carbon	1832	1.26	72	1.6	1343, 0.5 C	503, 800th, 2 C	758, 2 C	[104]
ZIF-8 & ZIF-67	N-doped Porous Carbon on Graphene	560	/	64	2.4	1372, 0.1 C	608, 300th, 1 C	786, 1 C	[105]
MOF-5	Hierarchical Pores Carbon Nanoplates	1645	1.18	54	/	1177, 0.1 C	730, 50th, 0.5 C	~850, 0.5C	[106]
MOF-5	GO@Meso-C	394	0.50	80	1.5	1122, 0.2 C	825, 100th, 0.2 C	550, 2 C	[107]
MOF-5	MWCNT@Meso-C	/	/	58	1.5	1343, 0.5 C	540, 50th, 0.5 C	/	[108]
MOF-5	Activated Meso-C Polyhedron	2211	2.62	79	/	1274, 0.2 C	1041, 50th, 0.2 C	441, 2 C	[109]

ZnFumarate	Hierarchical Pores Carbon	4793	3.99	55	/	1472, 400 mA g^{-1}	662, 40th, 400 mA g^{-1}	/	[110]
Basolite F300	Hollow Carbon Nano-Onions	514	1.01	~50	/	~1100, 2nd, 0.2 C	550, 40th, 0.2 C	/	[111]
Zn-MOF*[1]	Micro/Meso Porous Carbon Nanorod	1450	1.90	70	1.0–1.5	1210, 0.1 C	740, 200th, 0.5 C	850, 2 C	[112]
Zn-TDPAT	Flowerlike N-Doped Micro-C Nanosheets	1433	0.56	45	1.7	1645, 0.1 C	1220, 200th, 0.1 C 727, 1000th, 2 C	759, 5 C	[113]
Al-MOF*[2]	Hierarchically Porous Carbon Pillars	951	0.48	39–58	/	1466, 0.1 C (S: 50%)	524, 50th, 0.1 C (S: 50%)	236, 5 C (S: 50%)	[114]
Al-MOF*[2]	Porous Carbon	567	0.65	26−63	/	1273, 0.01 C (S: 46%)	419, 20th, 0.1 C (S:46%)	~900, 0.1 C (S: 46%)	[115]
Al-MOF*[2]	French Frieslike Hierarchical Porous Carbon	1124	1.00	58	1.0	1206, 0.1 C	856, 100th, 0.1 C	763, 2 C	[116]
Cu-MOF*[3]	Cross-linking Hierarchical Porous Carbon Fibers	1906	1.35	60	1.0–1.7	1336, 1 C	547, 500th, 2 C ~500, 500th, 5 C	801, 5 C	[117]
Cu 4,4′-bipyridine	Ultrahydrophilic Graphene Stacks	937	/	50	0.75	~1200, 0.1 C	~580, 100th, 1 C	~620, 2 C	[118]
Cu-BTC (HKUST-1)	Intertwined CNTs and Porous C Polyhedrons	1147	3.15	70	2.0−8.0	1290, 0.2 C (S: 2.0 mg cm^{-2})	855, 500th, 1C (S: 2.0 mg cm^{-2})	655, 10 C (S: 2.0 mg cm^{-2})	[119]
Cu-BTC (HKUST-1)	Nitrogen-Doped 3D Hierarchical Porous Carbon	730	0.81	74	/	1341, 0.5 C	695, 100th, 0.5C	349, 5 C	[120]

NOTE:
Micro-C: Microporous Carbon; Meso-C: Mesoporous Carbon.
*[1] Zn-MOF: $[Zn(bpdc)]_n$ (bpdc = 4,4′-biphenyldicarboxylate)
*[2] Al MOF: $Al(OH)(1,4\text{-}NDC)\cdot 2H_2O$
*[3] Cu-MOF: $[Cu(BTC\text{-}H_2)_2\text{-}(H_2O)_2]\cdot 3H_2O$

Table 3 Physical parameters and performances of MOF-derived carbon-metal composites as hosts for Li–S batteries.

Functional Species	Carbon-Based Framework	Precusor	Specific Surface Area	Total Pore Volume	Sulfur in Composite	Areal Sulfur Loading	Initial Discharge Capacity	Cycling Capacity	High-Rate Performing Capacity	Ref.
			$m^2\ g^{-1}$	$cm^3\ g^{-1}$	%	$mg\ cm^{-2}$	$mAh\ g^{-1}$	$mAh\ g^{-1}$	$mAh\ g^{-1}$	
Co–N	Graphitic Carbon	ZIF-67	309	/	70	2.0–2.5	1670, 0.05 C	850, 200th, 0.2C 625, 500th, 1C	656, 5 C	[121]
	Graphitic Carbon		282	/	52 (Li_2S)	2	1155, 0.2 C	930, 300th, 0.2C	373, 6 C	[122]
	RGO-Wrapped Graphitic Carbon		293	~0.31	59	1	1218, 300 mA g^{-1}	949, 300th, 300 mA g^{-1}	479, 5 A g^{-1}	[123]
	Honeycomb-Like Carbon		459	0.55	94	2.5–7.5	1674, 0.05 C (S: 3.6 mg cm^{-2})	514, 850th, 2 C (S: 3.6 mg cm^{-2})	290, 10 C (S: 3.6 mg cm^{-2})	[124]
	Graphitic Carbon Nanocages		182	0.28	77	2.0–2.3	1459, 0.1 C	718, 500th, 1 C	387, 2 C	[125]
	Nano-Porous Carbon		/	/	/	/	1030, 0.1 C	461, 500th, 0.5C	372, 2 C	[126]
	Graphene-Based Graphitic Carbon		/	/	25 (from EDX)	3.6	1459, 100 mA g^{-1}	673, 100th, 100 mA g^{-1}	410, 1000 mA g^{-1}	[127]
	CNTs Integrated Graphitic Carbon		496	0.38	71	2	1316, 0.1 C	970, 500th, 0.2C	674, 5 C	[128]
	CNTs Integrated Graphitic Carbon		653	2.06	76	5.2	1300, 0.1 C	860, 500th, 1 C	845, 2 C	[129]
	Carbon Fiber-Graphitic Carbon-CNTs Hybrid		744	1.55	75	1.5–13.5	1287, 0.2 C (S: 1.5 mg cm^{-2})	1060, 50th, 0.2C ~600, 2000th, 1C (S: 1.5 mg cm^{-2})	622, 10 C (S: 1.5 mg cm^{-2})	[130]

Table 4 Physical parameters and performances of MOF-derived carbon-metal compound composites as hosts for Li–S batteries.

Functional Species	Carbon-Based Framework	Precusor	Specific Surface Area	Total Pore Volume	Sulfur in Composite	Areal Sulfur Loading	Initial Discharge Capacity	Cycling Capacity	High-Rate Performing Capacity	Ref.
			$m^2\ g^{-1}$	$cm^3\ g^{-1}$	%	$mg\ cm^{-2}$	$mAh\ g^{-1}$	$mAh\ g^{-1}$	$mAh\ g^{-1}$	
Co_3O_4-N	RGO-Wrapped Graphitic Carbon	ZIF-67	273	0.93	75	2.1–5.9	1223, 0.2 C (S: 2.1 mg cm^{-2})	611, 1000th, 2 C (S: 2.1 mg cm^{-2})	652, 3 C, (S: 2.1 mg cm^{-2})	[131]
CoS_2-N	Graphitic Carbon	ZIF-67	/	/	69	1.2	1316, 0.2 C	600, 300th, 1 C	580, 2 C 268, 10 C	[132]
Co_3S_4	CNTs	ZIF-67	134	1.3	70	1.2–3.5	1535, 0.2 C (S: 1.2 mg cm^{-2})	752, 500th, 1 C (S: 1.2 mg cm^{-2})	702, 5 C (S: 1.2 mg cm^{-2})	[133]
Co_9S_8	3D Graphene Foam	Co-MOF	/	/	80–87	2.3–10.4	1306, 0.05 C (S: 2.3 mg cm^{-2})	736, 500th, 1 C (S: 2.3 mg cm^{-2})	670, 2 C (S: 2.3 mg cm^{-2})	[134]
$Al_2(OH)_{2.76}F_{3.24}$	CNTs - Porous Carbon	Al(OH)(1,4-NDC)·$2H_2O$	532	/	72	3.1	1563, 200 mA g^{-1}	719, 2000th, 2 A g^{-1}	~1000, 2 A g^{-1}	[135]
$Ti_3C_2T_x$ Mxene	Mesoporous Carbon	$Ti_3C_2T_x$ and MOF-5	1532	0.58	73	2.0	1226, 0.5C	704, 300th, 0.5C	544, 4 C	[136]
Mg/MgO	Mesoporous Carbon	Mg-BDC	310	0.77	69	~2	1201, 0.02 C	621, 200th, 0.2C	~220, 1 C	[137]
MnO_2	Meso-C	Al-MIL-101-NH2	1328 (Carbon)	0.7 (Carbon)	64	1.5–2.0	1475, 0.1 C	600, 450th, 1 C	452, 2 C	[138]
Ni_2P	Micro-C	MOF-74(Ni)	121	0.43	62	1.3–4.6	1357, 0.2 C	946, 300th, 0.2C	469, 5 C	[139]

3.1. MOF-derived carbons

3.1.1. Morphology control

To obtain better physisorption of polysulfides, morphology and porosity of carbon hosts should be well designed. These two characteristics are highly related to the precursor and the post-treatment methods. Compared to carbon hosts derived from other well-investigated precursors (e.g., sugars, celluloses and resins), morphology control of the MOF-derived carbons is more facile. Different morphologies from one-dimensional (1D) pillars/rods[114–117], two dimensional (2D) sheets [98,118] to three-dimensional (3D) complex architectures [100,103,104,113] can be synthesized by calcination of corresponding MOF precursors under inert atmospheres.

Wang et al. developed a 1D pillar-like hierarchically porous carbon by the thermolysis of Al-MOF (Al(OH)(1,4-NDC)·2H_2O). Due to the unique porous structure, excellent 5-C high-rate performance and cycle stability were achieved.[114] Following this work, Meng et al.[115] and Yang et al.[116] further investigated the sulfur anchoring capability of this Al-MOF-derived carbon materials. Yang et al. indicate that the improved polyculture confinement capability can be ascribed to the well-designed micro- and mesoporous structure.[116] In addition, the 1D conductive architecture also provided sufficient micropores for better Li-ion accessibility and established a conductive network for electron transfer. In a later work, Yang et al. designed another 1D porous carbon from a Cu-MOF (Cu(BTC-H_2)$_2$-(H_2O)$_2$]·3H_2O).[117] The as-obtained highly cross-linked structure allowed fast electron transfer. The hierarchical pore system can not only anchor polysulfide but also offer good Li-ion diffusion pathways. Consequently, an excellent high-rate performance of 515 mAh g^{-1} at 5 C was obtained even under a low working temperature of 0 °C.

2D MOF-derived porous carbon has also been developed. A multilayer graphene sheets stack, which is composed of well-preserved 2D sheets, was fabricated by Hao et al. via the thermal exfoliation of the copper 4,4′-bipyridine MOF.[118] The combination of the uniform morphology, hierarchical pores and highly polar N-doped carbon surface gave rise to an excellent performance as a sulfur host for Li–S batteries. Another novel 2D carbon was synthesized by Jiang et al.[98] By using a facile self-template method without organic solvent, monoclinic ZIF-8 nanosheets were prepared, which were transformed into hierarchically porous carbon after calcination.

3D carbon with photonic crystal architecture was proposed by Chen and Yang et al.[100] The unique architecture was produced via the nanocoating of ZIF-8 based on an assembled SiO_2 hard template. After the calcination and removal of the hard template, a 3D carbon with well-

defined large pores and sufficient meso- and micro pores was obtained (**Figure 6a&b**). The extremely high total pore volume of 13.42 cm^3 g^{-1} and large specific surface area of 2546 m^2 g^{-1} ensures the smooth ionic and electronic transfer. The cathode with 78 wt% of sulfur exhibited outstanding rate performance (**Figure 6c**) and cycle stability. Derived from a Zn-TDPAT precursor, a 3D flowerlike microporous carbon constructed by 2D carbon nanosheets was designed by Hong et al.[113] The combination of 2D and 3D structures promotes fast reaction kinetics and enables structural rigidity of the carbon framework. As a result, remarkable high-rate long-term 1000-cycle stability of 727 mAh g^{-1} was obtained at 2 C.

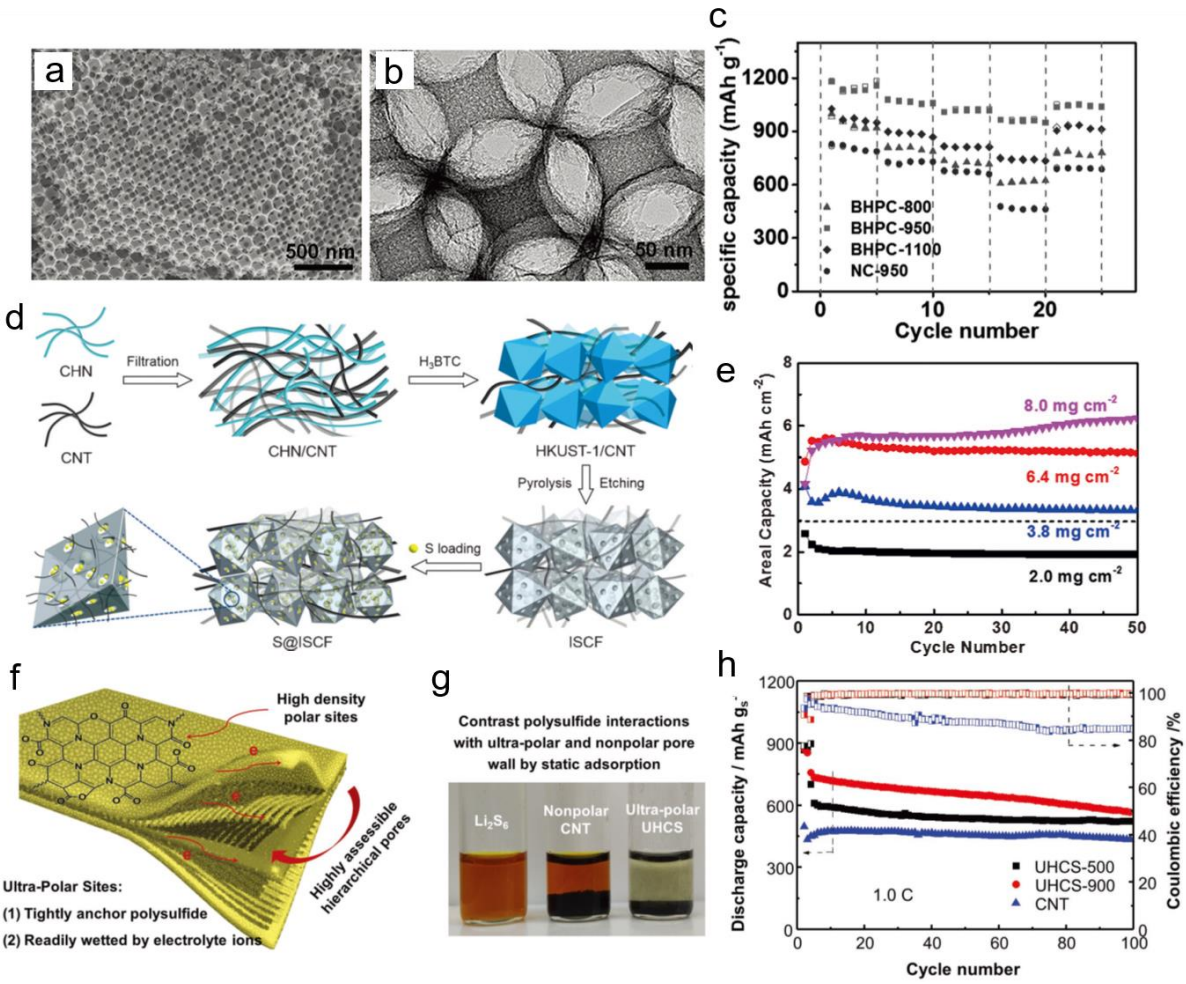

Figure 6 (a) SEM image and (b) TEM image of 3D carbon with photonic crystal architecture (BHPC-950) from ZIF-8; (c) Rate performance at 0.2, 0.5, 1 and 2 C of the cathode with 3D carbon hosts calcinated under different temperatures, (d) Illustration of the preparation processes of a S-C composite (S@ISCF) with MOF-derived carbon and highly conductive CNTs, (e) Cycling performances of S@ISCF cathodes with different areal sulfur loadings, (f) Schematic of advantages of ultra-hydrophilic graphene stacks (UHCS) as cathode host material, (g) Visualized comparison of polysulfide adsorption for CNTs and UHCS, (h) Cycling performances of the cathode with CNTs host and with UHCS host. Reprinted with permission from (a)-(c) [100] Copyright 2017 WILEY-VCH Verlag GmbH & Co. KGaA, Weinheim, (d), (e) [119] Copyright 2017 WILEY-VCH Verlag GmbH & Co. KGaA, Weinheim, and (f)-(h) [118] Copyright 2017 WILEY-VCH Verlag GmbH & Co. KGaA, Weinheim.

3.1.2. Pores modification

In a typical sulfur cathode, sulfur deposits in the form of ring-like S_8 molecules. Sulfur can also be infiltrated into hosts with ultra-small pores having a diameter less than 0.6 nm. In this case, the ring-like S_8 molecules would transform into short chain-like S_{2-4} molecules. These two types of sulfur would undergo distinguishable electrochemical process. As we illustrated in **Section 1**, the normal ring-like S_8 is reduced stepwise to high-order lithium polysulfides (Li_2S_n, $4 \leq n \leq 8$), low-order polysulfides (Li_2S_n, $n \leq 3$) and eventually Li_2S. In the reverse process, Li_2S is oxidized stepwise to S_8. However, owing to the space constraining of the ultra-small pores, small S_{2-4} molecules would prevent the generation of high-order polysulfides intermediates during redox reactions.[20] This indicates that the dissolving and shuttling of the high-order polysulfides could be prohibited.

MOF-derived microporous carbon is an ideal model system for explaining this feature. For example, Lou and co-workers proposed a ZIF-8 derived microporous carbon host.[90] When sulfur content was well controlled at 43 wt%, sulfur only deposited in the micropores. Therefore, excellent cycle stability was achieved. However, the S/C composite with excessive sulfur deposited on the surface of the MOF-derived host showed much inferior cell performance as well as stability. A few other works also designed microporous carbon materials from MOF precursors (e.g., ZIF-8 and Zn-TDPAT) and arrived at a similar conclusion that the small S_{2-4} molecules within ultra-small micropores can be well constrained after long cycling.[95,113]

However, hosts with ultra-small pores usually have very low pore volume, and therefore only a low content of sulfur (usually less than 50 wt%) can be loaded on these hosts. Typically, a Li–S battery cathode of more practical use would contain more sulfur (>70wt%) to ensure a decent energy density.[140,141] Well-controlled pore sizes of a MOF-derived carbon host can provide sufficient space for sulfur deposition, retain enough buffering for volume expansion of sulfur, and ensure smooth Li-ion diffusion pathways. Thus, the modification of pores is a useful strategy for improving performance of the cathodes with MOF derived carbon hosts.

Porous structures of MOF-derived carbon are highly associated with their MOF precursors. For example, Xi et al. compared four carbons from four different zinc-containing MOFs.[110] The as-obtained carbons have totally different specific surface areas varying from 969 to 4793 $m^2\ g^{-1}$, different pore volumes varying from 0.40 to 3.99 $cm^3\ g^{-1}$ and different pore size distributions. Carbon host from ZnFumarate MOF showed the best sulfur utility and cycle stability due to the high porosity and proper pore size distribution.

For a specific MOF precursor, the porous structures of MOF-derived carbon can be tuned by approaches like calcination temperature alteration[102,109,111], KOH activation[98,109], gas

etching[97], and hard-templating[96,117]. Generally, a lower calcination temperature leads to a higher surface area and a larger pore volume in the MOF-derived carbon. Klose et al. calcined Basolite F300 MOF at 800, 900 and 1000 °C to obtain graphitic carbon. The carbon host generated from calcination at 800 °C displayed better performance.[111] Cai et al.[109] indicated in a later report that an optimized carbonization temperature should be evaluated. Using MOF-5 as a precursor, they found that the highest porosity was achieved at 950 °C when the calcination temperature varied from 900 to 1000 °C. A better charge transfer as well as performance were observed on the cathode with the host calcinated at 950 °C. A similar result was also observed by Zhang et al.[102] On the basis of an optimal calcination temperature, the molten KOH salt can further enhance the porosity. After a post-treatment of molten KOH, carbons derived from both MOF-5 and ZIF-8 delivered improved performances.[98,109]

Post-treatment using ammonia (NH_3) atmosphere was proposed by Li et al.[97] After a 1000 °C calcination, a microporous ZIF-8 derived carbon was obtained. After a NH_3 etching at 1100 °C for 3 min, a significant rise of the micro porosity was observed, which was accompanied with a small amount of mesopores. The resultant carbon with hybrid pores presented much improved cycle stability within a 1000-cycle performance. Further treatment under NH_3 led to the formation of a hierarchically porous structure, with a total pore volume doubled relative to the untreated ZIF-8 derived carbon.

Self-sacrificing template method was proposed by Ding et al.[96] In their work, ZIF-8 was in situ grown on porous ZnO nanosheets, followed by a further calcination treatment. During the calcination, ZnO was reduced and evaporated, resulting in the production of a carbon material with micro- and mesopores. The cathode with the novel carbon host exhibited advanced performances. In a following work by Chang et al., a multilayered carbon matrix was also generated via the ZnO assisted synthesis.[104] An analogous self-sacrificing approach was also reported on a Cu-MOF, which involves the removal of Cu particles to produce porous carbon.[117] Hard-templating methods using 3D close-packed SiO_2 as the template were also proposed to get carbon materials with a photonic crystal architecture.[100]

3.1.3. Hybridization

Hybridization of MOF-derived carbon with other functional reagents like graphene oxide (GO), reduced graphene oxide (rGO) and carbon nanotubes (CNTs) can further aid the sulfur confinement and the long-range electron transport. Bao et al. integrated GO sheets into the MOF-5 calcination process.[107] An efficient electronic transfer and Li-ion diffusion pathway was beneficial to the high-rate performance of the sulfur cathode. Chen et al. wrapped the

sulfur/carbon composite with graphene by a facile ultrasonic method.[94] Liu et al. reported a self-standing host integrating HKUST-1 derived porous carbon polyhedrons and CNTs (**Figure 6d**).[119] Strong coupling between the porous carbon and the highly conductive CNTs offers excellent long-range electron transfer pathways. Consequently, outstanding high-rate performance of 655 mAh g^{-1} was recorded at 10 C. The unique free-standing architecture also makes it possible to load ultra-high amount of sulfur. A high areal capacity of more than 6 mA cm^{-2} was achieved with a cathode with high areal sulfur loading of 8.0 mg cm^{-2} (**Figure 6e**). Another work that hybridized CNTs with MOF-5 derived carbon to improve the rate capacity was reported by Bao et al.[108] A rationally designed hybrid with CNT, porous carbon and rGO was proposed by Song et al.[101] The in situ grown ZIF-8 on CNTs allowed good contact between the MOF-derived carbon and the CNTs, which is beneficial to the electron transfer. In addition, the rGO wrapping serves as diffusion barriers for immobilizing polysulfides. Another hybrid comprising rGO, ZIF-8 derived carbon and PEDOT was presented by Tan et al.[99] They indicated that further wrapping of PEDOT provides additional capability of sulfur anchoring, leading to enhanced cycle stability. Very recently, Chen et al. reported a N-doped porous carbon anchored graphene composite by in-situ growing ZIF-8 (Zn) and ZIF-67 (Co) on GO followed by calcination.[105] The particle sizes and morphologies of the composites are highly associated with the initial ratio of Zn^{2+} and Co^{2+} in the preparation process. The facilitated sulfur utilization and electronic transport could be ascribed to the interconnected graphene framework.

3.1.4. Nitrogen doping

A systematic DFT calculation proposed by Hou et al. compared different heteroatoms-doped carbons. They proved that N dopant, especially pyridinic nitrogen, can enhance the surficial interaction between carbon hosts and polysulfides.[142] Hong et al applied the N-doping strategy to the Zn-TDPAT derived carbon.[113] They concluded that the pyridinic, pyrrolic, and pyridone N provide polysulfide binding sties while the graphitic N improves the electrical conductivity of the carbon. The proper nitrogen content in the carbon and the unique 3D porous architecture synergistically facilitate the performance of the cathode. Hao et al. suggested that the polar surface of the N-doped MOF-derived carbon also offered a better wettability to electrolyte, which can facilitate the ionic diffusion process (**Figure 6f**).[118] Visualized comparison (**Figure 6g**) of polysulfide adsorption revealed the strong interaction between the polar surface of the N-doped carbon and the polysulfides. The combination of good electrical conductivity, strong surface interaction with polysulfides and the decent electrolyte wettability

contributes to the good performance and stability of the cathode (**Figure 6h**). The positive effects of N doping on the electronic and ionic transport and surface chemical interaction to polysulfides are also demonstrated by some other works.[95,99–101,120] Zhang et al. recently conducted a systematic study on the correlations between calcination temperature, porosity and nitrogen content of the MOF-derived carbon.[102] They pointed out that a high N-doping content would not definitely lead to good performance. A sufficient surface for chemical interaction is also essential to the high performance of the cathode.

As we demonstrated in **Figure 1c&d**, the electrical conductivity, porosity, and surface chemisorption to polysulfides are essential parameters to hosts for Li–S battery cathode. The N-doping of the MOF-based carbon materials can provide additional chemisorption capability.

3.2. MOF-derived carbon-based composites

3.2.1. MOF-derived carbon-metal composites

As demonstrated in **Figure 5**, the chemisorption of polysulfides with MOF-derived carbon-based metal/metal compound composites is higher than those with MOF-derived carbons. The evenly dispersed metal nodes in MOF precursors can facilely transform into metal or metal compound particles after calcination. One of the well-investigated transition metal-containing precursors is ZIF-67 which produces Co nanoparticles decorated, N-doped graphitic carbon (Co–N–GC) composites. As illustrated in **Figure 7a**, a typical synthesis of Co–N–GC includes calcination at high temperature (800−1000 °C) under inert atmosphere[121,122,127] or at mediumtemperature (500−600 °C) under reductive H_2/Ar atmosphere[123,125].

A pioneering work was proposed by Dong and co-workers.[121] By in-situ converting a Co and N containing ZIF-67 precursor, both doped N and metallic Co particles were incorporated in the graphitic carbon. The nitrogen atoms, especially pyridinic N, provided strong binding of polysulfides via Li-N interaction. An excellent reversible capacity of 625 mAh g^{-1} was retained after 500 cycles at 1 C (**Figure 7b**). On the contrary, the sample prepared by physically mixing cobalt with ZIF-8 derived N-doped graphitic carbon (Co/ACN) presented a much inferior result, even though the high adsorption capability to polysulfides of both samples was similar (**Figure 7c**). The strong interaction between polysulfides and the Co–N–GC matrix was further confirmed later using DFT calculation (**Figure 7d**) by He et al.[122]

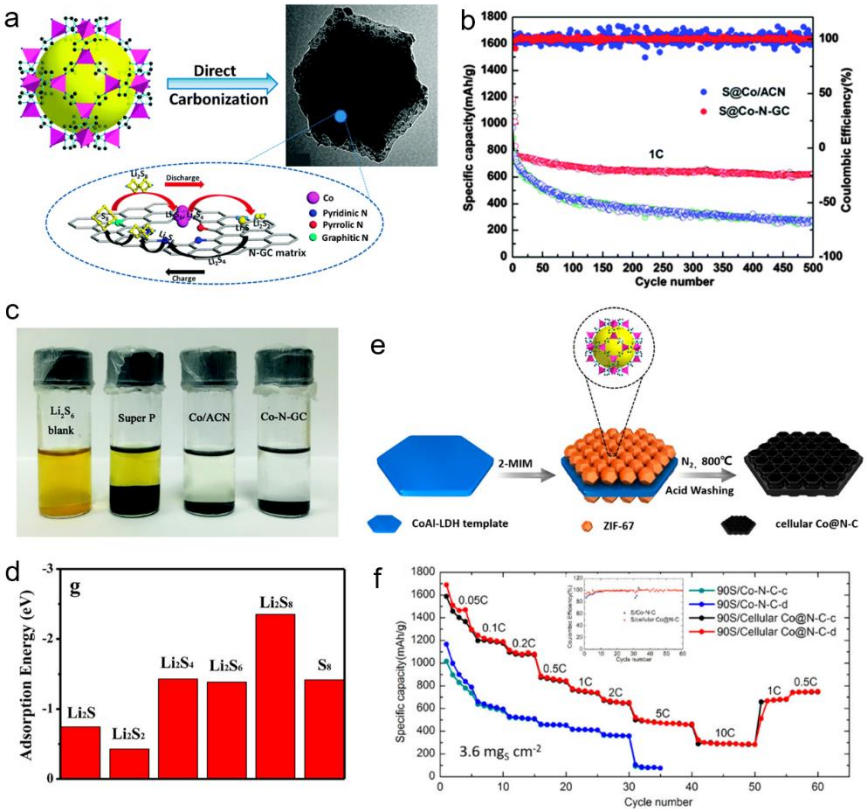

Figure 7 (a) Illustration of the preparation of ZIF-67-derived Co–N–GC and its interaction with polysulfides in a working Li–S battery cathode, (b) Cycle stabilities of S@Co–N–GC and S@Co/ACN composites at 1C, (c) Visible comparison of Li_2S_6 solutions after contacting with different hosts, (d) DFT computation result of adsorption energy for lithium polysulfides on C−Co−N, (e) Illustration of the synthetic process of cellular Co@N−C, f) Rate performances of the cathode with cellular Co@N−C and Co−N−C hosts, with Coulombic efficiency shown in the inset. Reprinted with permission from (a)–(c) [121] Copyright 2016 Royal Society of Chemistry, (d) [122] Copyright 2016 American Chemical Society and (e), (f) [124] Copyright 2017 American Chemical Society.

The aforementioned two works also demonstrated the synergistic catalytic effect of Co–N in facilitating the redox reactions of sulfur species **(Figure 7a)**.[121,122] On the one hand, cobalt particles enable the conversion of high-order polysulfides to low-order ones during the discharge process, which improves the depth of the sulfur reduction and thus leads to better sulfur utilization. On the other hand, nitrogen atoms in the graphitic carbon promote the sulfur oxidation during the charging process. The Improvement of sulfur utility and cycle performance by this catalytic effect is confirmed by experimentally comparing hosts with or without Co and N decoration. Even though the improved sulfur redox kinetics and stabilities have been verified by electrochemical evidence, the mechanisms behind the catalytic effect of cobalt and/or cobalt-nitrogen are still not well understood. Further investigation might clarify this issue in the future.

The cell performances and cycle stabilities of the Co–N–GC host were further promoted by other extended designs like engineering integration with other functional reagents[123,127] and rational design of novel architectures [124]. The integration of RGO nanosheets can establish an additional barrier layer [123] or construct well-contacted conducive frameworks [127]. To

enlarge the energy density of the Co-N-C cathodes, Dong and co-workers designed a honeycomb-like quasi-2D Co@N−C composite (**Figure 7e**).[124] The highly porous cellular flake and honeycomb structure can accommodate a high sulfur content of 93.6 wt%. A very high areal loading of sulfur up to 7.5 mg cm^{-2} on cathode was achieved by simply stacking the flakes. By taking advantage of the unique sulfur anchoring and catalytic effect from Co–N–GC as well as the rationally designed architecture, excellent rate and cycling performance was achieved at a current density up to 10 C (**Figure 7f**). Very recently, ZIF-67 derived Co@N−C composites were integrated with different in-situ catalytically grown CNTs by serval groups.[128−130] For example, Li et al. designed a stringed "tube on cube" nanohybrid consisting of carbon fiber skeleton, ZIF-67 derived porous graphitic carbon, and CNT tentacles.[130]. The sulfur composite with the unique nanohybrid host demonstrated excellent 10-C high-rate cyclability for 2000 cycles.

3.2.2. MOF-derived carbon-metal compound composites

To maximize the chemical adsorption to polysulfides, a wide range of metal compounds have been utilized as polar hosts without a carbon-based framework. Serving as self-sacrifice templates, MOF materials are ideal metal compound precursors. Metal compounds with special morphology and highly porous structure can be produced by well-controlled etching or combustion of MOFs. An outstanding attempt was made by Lou and co-workers, where ZIF-67 derived double-shelled $Co(OH)_2$/LDH nanocages were designed as efficient host materials.[143] As illustrated in **Figure 8a**, ZIF-67 first reacted with $Ni(NO_3)_2$ in ethanol forming a Ni-Co LDH external shell. Then the material was further treated with Na_2MoO_4 in an ethanol/water mixture forming a $Co(OH)_2$ inner shell. This double-shelled hollow structure with self-functionalized polar surfaces offered efficient dual confinement of polysulfides. The cathode with 75 wt% of sulfur demonstrated improved performance compared to a mesoporous carbon/sulfur cathode (**Figure 8b**). However, the high-rate performance was limited up to 1 C (**Figure 8c**), which still cannot compare favorably to other advanced hosts with high electrical conductivity. A simpler route for the synthesis of hierarchically porous TiO_2 was proposed by Li et al.[144] The excellent cycle stability (675 mAh after 500 cycles at 1 A g^{-1}) indicates the effective dual confinement of polysulfides by the hierarchically porous structure and the chemical TiO_2-S_x interaction.

It is noted that most of the typical carbon-free MOF-derived compounds (e.g. $Co(OH)_2$, TiO_2, ZnO, CuO) have low electrical conductivity similar to their MOF precursors. Considering that both MOFs and MOF-derived metal compounds have decent chemisorption capability to polysulfides, it seems that further synthetic steps have not brought about many benefits to

optimized materials. This might explain the fact that only a few works have focused on producing metal compounds without a carbon-based framework for Li–S batteries so far.

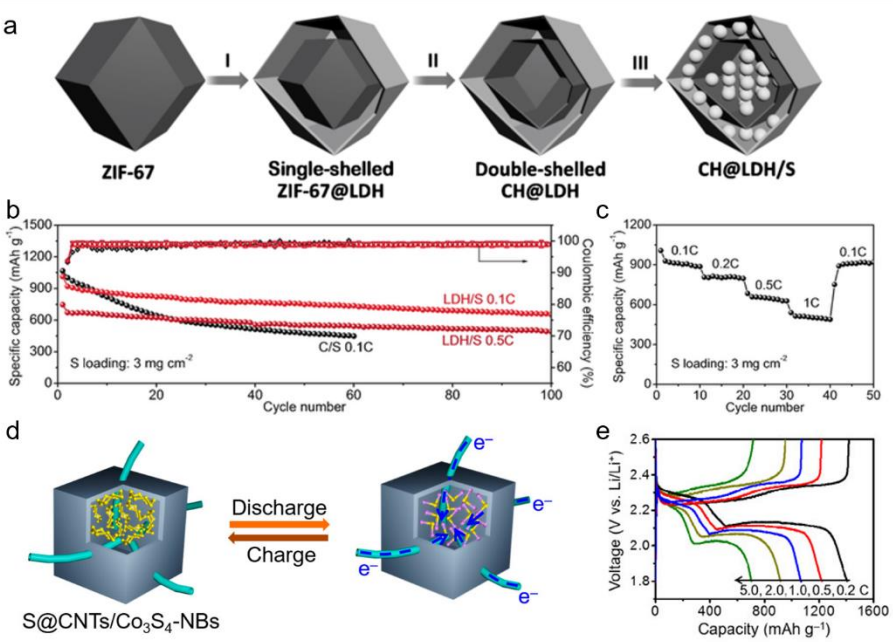

Figure 8 (a) Illustration of synthetic procedures of cobalt hydroxide @ layered double hydroxides - sulfur cathode (CH@LDH/S), (b) Cycle performances of CH@LDH/S and C/S, (c) Rate performance of CH@LDH/S with the current range of 0.1–1C, (d) Illustration of the structural advantages of S@CNTs/Co_3S_4−NBs cathode during performance, (e) Discharge-charge profiles of S@CNTs/Co_3S_4−NBs at different current densities. Reprinted with permission from (a)–(c) [143] Copyright 2016 WILEY-VCH Verlag GmbH & Co. KGaA, Weinheim, (d), (e) [133] Copyright 2017 American Chemical Society.

In order to fully take advantage of the high pore volume and uniform morphology of a MOF-derived metal compound, developing highly conductive metal compounds like Ti_4O_7 [145,146] and CoS_2 [43,147] and embedding MOF-derived compounds in a MOF-derived carbon could be a good strategy. Liu and Jin et al. designed hollow Co_3S_4 nanoboxes interlaced by CNTs. The intrinsically conductive Co_3S_4 nanoboxes served as a sulfur confinement unit due to the chemical adsorptive surface. The interconnected CNT frameworks created excellent long-range electron transfer pathways (**Figure 8d**). The cathode with 70 wt% of sulfur obtained an excellent high-rate reversible capacity of 702 mAh g^{-1} up to 5 C (**Figure 8e**). Very recently, Manthiram and co-workers designed a 3D graphene foam supported Co_9S_8 composite.[134] Co-MOF was first grown on the 3D graphene foam and was then subjected to sulfurization by thioacetamide. The cathode with 3D Co_9S_8-graphene host delivered excellent performance even with a very high sulfur loading of 10.4 mg cm^{-2}. In addition, further oxidization of a calcined ZIF-67 matrix to produce a Co_3O_4–N–C/GO composite also gave rise to a great cycling performance, which is due likely to the dual binding effect between polysulfides and Co_3O_4, that is, the strong ionic Li–O bonds and the Van der Waals attractions between S and Co.[131] In the case of CoS_2–N–C obtained by sulfurization of Co-N-C matrix, a similar dual binding

effect was observed.[132] Recently, a novel complex with CNTs, MOF-derived carbon and $Al_2(OH)_{2.76}F_{3.24}$ was developed by Li et al.[135] With a hydrogen fluoride treatment, The Al-MOF derived Al_2O_3 transformed into $Al_2(OH)_{2.76}F_{3.24}$ which showed excellent chemical immobilizing of polysulfides. The cathode with the CNTs/MOFs-derived carbon/$Al_2(OH)_{2.76}F_{3.24}$ host exhibited excellent cycle stability within the ultra-long 2000 cycles. A Mg/MgO containing carbon-based host was also proposed by calcining the Mg−1,4-BDC MOF precursor.[137] The good performance was attributed to the embedded Mg that enhances electrical conductivity and the MgO that provides chemisorption to polysulfides. Very recently, a Ni_2P embedded microporous carbon composite was reported by Cheng et al.[139] Decent polysulfides anchoring with high areal sulfur loading of up to 4.6 mg cm^{-2} was achieved due to the well-constructed 3D conductive network with well dispersed polar Ni_2P nanoparticles.

In afore-mentioned reports, metal or metal compound particles were obtained via the transformation of metal ligands in the MOF precursors. Another route to synthesize metal compound-carbon composites was designed by Bao et al.[136] Novel exfoliated Mxene material (Ti_3C_2Tx, $Tx \approx F_xO_y$) was directly integrated into a MOF-derived carbon. Compared to other Mxene sulfur hosts reported earlier by Nazar and co-workers,[148] the well-dispersed MXene around the MOF-derived carbon prevented the restacking of the exfoliated Mxene, thereby achieving better ionic accessibility. As confirmed by XPS and computational analysis, the hydrophilic surfaces of the Mxene@Meso-C offered excellent chemisorption for polysulfides. The mesoporous structure derived from the MOF-5 precursor further enhanced the sulfur utility and confinement. As a result, impressive performances and stabilities of the Mxene-carbon-sulfur composite were observed. In another work, MnO_2 and graphene were combined with the MOF-derived carbon and good cycle stability was obtained.[138] Recently, a non-metal polar compound consisting of g-C_3N_4 nanodots was also embedded into a NH_2-MIL-101(Al) derived carbon to construct a novel host for Li–S battery.[149]

3.3. A brief summary

MOF-derived materials obtained by calcination of MOFs offer an alternative approach for intrinsically improving electrical conductivity of the host and simplifying the chemical interaction of the cathode system. The pore volume and surface sulfur chemisorption capability are predominant factors that determine the capability for sulfur storage, sulfur utility and sulfur confinement.

Porous carbon with different morphologies can be facilely synthesized by inheriting the morphological features and highly porous structures of the MOF precursors. Sulfur undergoes

two distinguishable electrochemical processes for carbons with different pore size distributions. Porous structures can be tuned by approaches like calcination temperature alteration, KOH activation, gas etching and hard-templating. Hybridization of MOF-derived carbon with other functional reagents like GO, rGO and CNTs can further facilitate the sulfur confinement and the long-range electron transport. Nitrogen doping of MOF-derived carbons further improves the intrinsic conductivity of the carbon host and provides additional surface chemisorption to polysulfides.

MOF-derived carbon-metal composites and carbon-metal compounds composites can lead to improved performances and stabilities. This is ascribed to the high chemisorption that is comparable to that of MOF-based hosts, as well as the high intrinsic electrical conductivity of the carbon frameworks. Nano transition metal particles incorporated in a MOF-derived graphitic carbon may provide an attractive catalytic effect on sulfur reduction, benefiting the extent of sulfur utilization. While MOF derived carbon-free metal compounds are rarely studied, well-designed MOF-derived metal compounds can still offer decent cycle stability due to the highly porous structure and the strong chemisorption to polysulfides. Well-dispersed metal compounds (e.g., oxide, sulfide and Mxene) coupled with MOF-derived carbon can combine the benefits of good electrical conductivity, high porosity and strong chemical anchoring of polysulfides, and are thus expected to show excellent performance and cycle stability.

4. Functional barriers for polysulfides

Commercially available separators for lithium batteries depart anode and cathode to prevent short circuit, and at the meantime, provide micro channels for ion diffusion. However, dissolved polysulfides can easily penetrate through most of the commercial separators (**Figure 9a**). To alleviate the shuttle of polysulfides, a new battery configuration with an additional functional interlayer between cathode and anode was first proposed by Manthiram and co-workers in 2012.[59,60] Based on this configuration, barriers with porous MOF-derived carbon and adsorptive metal compounds adsorb and reutilize the polysulfide within the porous and electron conductive film.[150−153] We refer to this strategy as an “adsorbing-reutilization approach”. In 2016, a novel “blocking approach” was proposed, where a dense, electron insulating MOF film was discovered for blocking polysulfide.[61,154] Some of the functional barriers and their performances are presented in **Table 5**, where two different strategies for polysulfide resistance are demonstrated.

Table 5 Performances of Li–S batteries with functional polysulfide barriers.

Sulfur Resisting Strategy	Material	Sulfur in Cathode Composite	Areal Sulfur Loading	Initial Discharge Capacity	Cycling Capacity	High-Rate Performing Capacity	Ref.
		%	mg cm^{-2}	mAh g^{-1}	mAh g^{-1}	mAh g^{-1}	
Adsorbing-Reutilization Approach	TiO_2@NC	80	/	1435, 0.2 C	712, 500th, 1C	736, 3 C	[150]
	N–C–Co Film	~75	1.5–5.2	~1600, 0.2 C	660, 250th, 1C	779, 5 C	[151]
	Co_9S_8 Hollow Nanowall Arrays	100	2.0–5.6	1385, 0.1 C (S: 2 mg cm^{-2})	1190, 200th, 0.1 C 530, 1000th, 1 C (S: 2 mg cm^{-2})	428, 2 C (S: 2 mg cm^{-2})	[155]
	Ni-MOF-74@CNTs	60	2.0	1358, 0.2 C	1183, 300th, 0.2 C	968, 2 C	[152]
	ZIF-8 @CNTs	70	1.2	1655, 0.1 C	870, 100th, 0.2 C	583, 2 C	[153]
Blocking Approach	HKUST-1	70	0.6–0.8	~1200, 0.1 C	855, 1500th, 1 C	488, 3 C	[61]
	Zn-HKUST-1	70	0.6–0.8	1118, 1 C	657, 1000th, 1 C	/	[156]
	ZnPTz @Carbon Fiber Paper	100	3.5–9.6	1416, 0.1 C (S: 3.5 mg cm^{-2})	~1000, 50th, 0.1 C (S: 9.6 mg cm^{-2})	859, 2 C (S: 3.5 mg cm^{-2})	[157]
	Y-FTZB@CNTs	70	1	1480, 0.1 C	557, 300th, 0.25 C	~450, 2.5 C	[158]
	Zn_2(benzimidazolate)$_2$($OH)_2$	70	1.0	1407, 0.1 C	738, 200th, 0.25 C	610, 2.5 C	[154]
	Mn-BTC	65	/	1430, 0.1 C	~1100, 80th, 0.1 C	900, 1 C	[159]
	UiO-66-NH_2@SiO_2	75	0.5	1400, 0.1 C	~600, 100th, 0.1 C	/	[160]
	PSS@ HKUST-1	~70	1.3–11.3	1331, 0.2 C (S: 1.3 mg cm^{-2})	775, 500th, 0.5 C (S: 1.3 mg cm^{-2})	423, 5 C (S: 1.3 mg cm^{-2})	[161]

4.1. Adsorptive interlayers

As demonstrated in **Section 3**, MOF-derived materials which usually have highly porous structure and adsorptive capability to polysulfides can be used as an efficient interlayer based on the "adsorbing-reutilization approach". A ZIF-67 derived N–C–Co interlayer which is attached to S/C cathodes (**Figure 9b**) was developed by Wang et al.[151] The highly porous, nitrogen-doped carbon structure offers both good physisorption and chemisorption to the dissolved polysulfides from the cathode. The adsorbed sulfur could be well reutilized due to the high electrical conductivity of the interlayer. A good initial capacity of ~1600 at 0.2 C was observed, indicating the effective adsorption and utilization of sulfur from integrating the N–C–Co interlayer. Since the shuttling of polysulfide was well suppressed, excellent cycling

performance with a capacity of 660 mAh g^{-1} after 250 cycles at 1C was obtained. The cathode with an aerial sulfur loading up to 5.2 mg cm^{-2} also demonstrated excellent cycle stability. Based on a similar configuration, An et al. proposed a NH_2-MIL-125(Ti) derived TiO_2 on N-doped carbon composite as the interlayer for Li–S batteries.[150] The ultrafine TiO_2 incorporated on the porous conductive network and the N-doping of the carbon enabled dual chemisorption for anchoring polysulfide. Consequently, improved rate performance and prolonged cycling stability was realized. Very recently, Manthiram and co-workers demonstrated a strategy that coated a commercial separator with multifunctional Co_9S_8 polar interlayer.[155] The vertical Co_9S_8 hollow nanowall arrays with high electronic conductivity presented a significant enhancement of the performance, reaching an average capacity fading rate of 0.039% per cycle over 1000 cycles at 1 C.

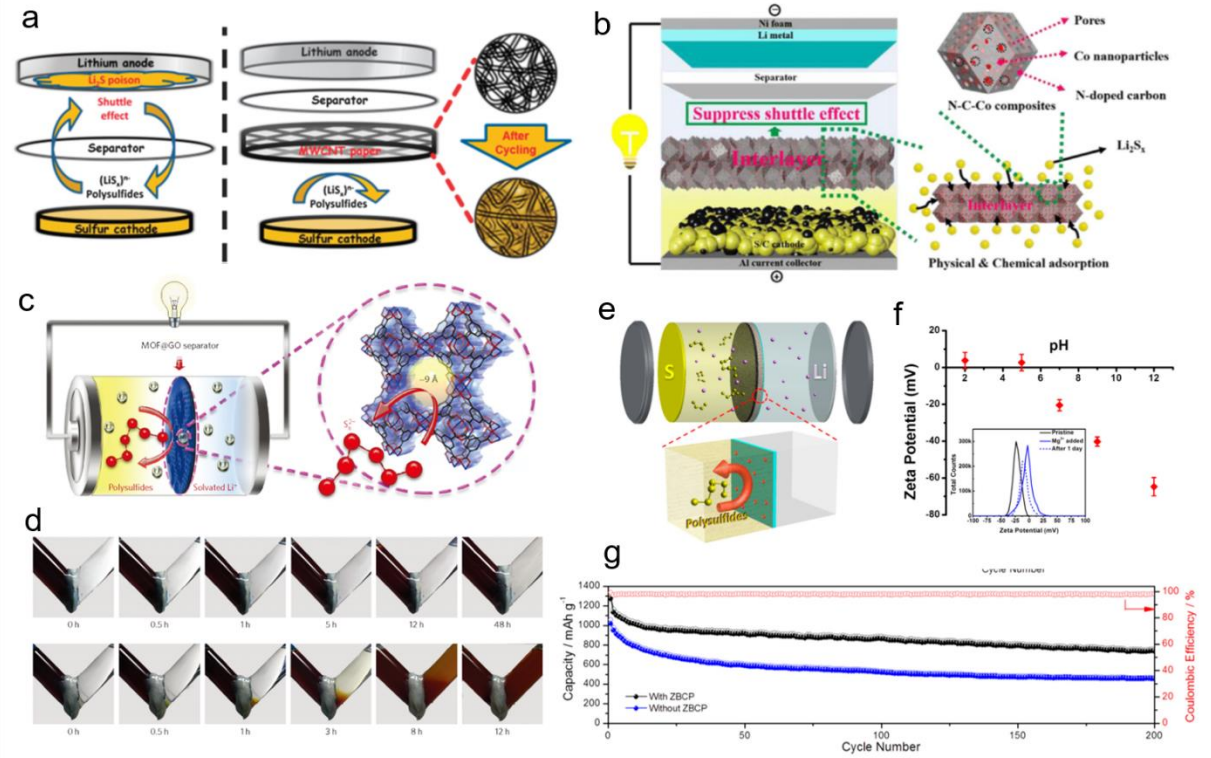

Figure 9 Functional polysulfide barriers based on the adsorbing-reutilization approach and the blocking approach. (a) Traditional Li–S battery configuration and configuration with a porous MWCNT interlayer for adsorbing and reutilization of dissolved polysulfides, (b) Li–S battery with a MOF-derived porous N–C–Co composite interlayer, (c) Polysulfide blocking separator composed of GO and dense MOF with well-defined pore size of 9 Å, (d) Polysulfide permeation comparison of a MOF@GO separator (top) and a GO separator (bottom), (e) Polysulfide blocking separator with a negatively charged surface, (f) Zeta potentials of aqueous dispersion with ZBCP particles with various pH (The inset shows the zeta potential variation after adding Mg^{2+}), (g) Comparison of cycle stability of Li–S batteries using separators with and without ZBCP charged coating at 0.25 C. Reprinted with permission from (a) [60] Copyright 2012 Royal Society of Chemistry, (b) [151] Copyright 2018 Elsevier, (c),(d) [61] Copyright 2016 Springer Nature, and (e)–(g) [154] Copyright 2018 American Chemical Society.

4.2. Blocking separators

A novel alternative configuration that blocks polysulfides with a dense MOF "wall" was first proposed by Zhou and co-workers in 2016 (**Figure 9c**).[61] HKUST-1 MOF layer was in-situ grown on a filter paper, then GO was covered on the MOF layer by filtration. This MOF-based separator served as an ionic sieve in Li–S batteries. The well-defined micropores (aperture of ~9 Å) on the MOF are smaller than the diameters of soluble polysulfides. Lithium ion with a much smaller diameter can go through the aperture. The excellent blockage effect is confirmed by permeation experiment illustrated in **Figure 9d**. A Li–S battery with the MOF@GO separator demonstrated a remarkable cycle stability with a fading rate of ~0.019% over 1500 cycles. An subsequent work by Zhou and co-workers demonstrated that a separator with Zn-HKUST-1 also presented excellent polysulfide blocking.[156] This work further discussed the structural and chemical changes of HKUST-1 and Zn-HKUST-1 during cycling. A later work by Li et al. found that the packing density of the MOF particle also has a vital influence on the performance of polysulfide blockage.[158] This publication also notes that the degradation of MOF may occur during cycling, hence a suitable voltage window should be carefully applied.

Most recently in 2018, another distinctive strategy for blocking polysulfides, which is via the construction of a negatively charged shield, was showcased by Huang et al. (**Figure 9e**).[154] They proposed a free-standing 2D coordination polymer (Zn_2(benzimidazolate)$_2$$(OH)_2$) without well-defined pore structure. Due to the stoichiometrically coordinated –OH groups on the Zn nodes, the polymer is intrinsically negatively charged (**Figure 9f**), thus providing unique resistance to polysulfides (negative anion). As a consequence, much enhanced sulfur utility and cycle stability were observed for batteries with the barrier (**Figure 9g**). A similar polysulfide resisting effect was observed for a Mn-BTC MOF reported by Suriyakumar et al.[159] With a negatively charged surface due to the COO^- functional groups, polysulfides which are also negatively charged are repulsed. Therefore, a greatly improved performance and stability was achieved.

A design that combines both adsorbing-reutilization approach and blocking approach was proposed by Chiochan et al.[157] The interlayer consisted of an oxygen functionalized carbon fiber as frontside toward the cathode and a dense ZnPTz layer as backside toward the anode. As proved by DFT investigation, both faces of the interlayer favored efficient polysulfide chemisorption. In addition, the dense, nonporous backside of ZnPTz also served as a physical shield for sulfur blocking.

4.3. A brief summary

Improved sulfur utility and cycle stability can be achieved by developing new battery configurations. Two different types of polysulfide barriers have been proposed to tackle the shuttling of polysulfides. The polysulfide barriers based on adsorbing-reutilization approach and the blocking approach can effectively prevent the penetration of polysulfides between the cathode and anode. The physical and chemical adsorption capability and the conductivity are essential parameters for barriers based on the polysulfide adsorbing-reutilization approach. The aperture window size of the MOF, the surface charge status, the packing density of the particle and the stability during cycling are predominant factors for barriers based on the polysulfide blocking approach.

5. Conclusion and perspectives

In this review, the advanced strategies for designing MOF-based and MOF-derived materials as hosts and polysulfide barriers for Li−S batteries are summarized. Exciting progress on developing new MOF-based and MOF-derived materials as hosts and as polysulfide barriers for high-performance Li−S batteries has been made over the last few years. Till now, essential parameters for the design of new MOF-related hosts and the correlations between each parameter are clarified.

As we indicated in **Figure 1c**, sufficient porosity, high electrical conductivity and decent surficial chemisorption capability to polysulfides are vital for an advanced host for sulfur. The porosity of the host is the prime parameter to consider. A large pore volume is essential for sulfur deposition. Sufficient pores are also important to smooth Li-ion diffusion, which is beneficial to the high-rate capacity. Furthermore, high porosity could also alleviate the diffusion of polysulfides through a physical capillary adsorption. It can also buffer the volume change of sulfur during cycling, thus enhancing cycle stability. Based on a sufficient porosity, hosts with high electrical conductivity can facilitate the electron transfer, which is vital to the improvement of rate performance. Also of importance is the additional strong surficial chemical interactions between hosts and polysulfides, which can contribute to long cycling stability.

Even though tremendous advances have been achieved to successfully developing new MOF-related materials and discovering the mechanism behind the improved Li−S battery performances, substantial challenges still remain to be overcome.

A common drawback of the direct utility of MOFs as host is the low electrical conductivity. Generally, the best high-rate performances of the cathodes with MOF-related materials are still hardly comparable to those with ultra-high rate performance up to 20 C of the most excellent

carbon-based hosts such as graphene and CNT.[32,162,163] Therefore, the development of highly conductive MOFs or new compositional designs which integrate MOF-based materials with advanced highly conductive materials for Li−S batteries are highly expected. In addition, further investigation should identify promising metal nodes and optimize their chemical states (e.g., valence, coordination). Furthermore, a mechanistic understanding of the influence of metal nodes on the extent of sulfur reduction and on the redox kinetics is still lacking. Unlike well-investigated oxygen reduction reaction and oxygen evolution reaction, the conversion process between S_8 and Li_2S is much more complicated.[164] More experimental study based on advanced characterizations is necessary to offer more insights into the role of metal nodes, which could guide the development of novel multifunctional MOFs. Moreover, a few reports on MOF-based hosts or interlayers indicate that metals or organic ligands in MOFs may react with lithium or sulfur during cycling.[58,158,159] Future work should focus on the structural and compositional stabilities of different MOFs during long-term battery cycling. Possible safety issues should also be identified and addressed in the future, especially for batteries working under a wide temperature range.

For MOF-derived hosts, there is much room for the improvement of the volume energy density of Li−S batteries with the MOF-derived host. A drawback of the sulfur cathode lies in its relatively low volume energy density compared to other metal compound cathode materials. This issue would become even more problematic when highly porous MOF-derived hosts are adopted. Future development of hosts should be able to provide a solution to tackle this issue.

Dense polysulfide barriers composed of MOFs can effectively resist the penetration of polysulfides. At the same time, however, the lithium diffusion pathway might be hindered. As already observed in solid-state lithium batteries,[165] MOF may serve as a solid lithium conductive electrolyte.[166] Therefore, more investigation should be conducted to reveal how lithium diffuses through the dense MOF blocking layer.

Lastly, it is worth mentioning that MOF-derived materials also demonstrate noticeable performance improvement in other alkaline chalcogenides battery systems such as room-temperature non-aqueous Na–S batteries [167,168], Li–Se [169–171] and Na–Se [172] batteries which are also suffering from a similar cathode dissolving issue.

Overall, the development of new MOF-derived materials or MOF-based materials is still in its infancy. Overcoming the challenges above would deepen our understanding of this burgeoning field of research. However, it would be still far away from the practical use of MOF-related materials in a commercially competitive battery system. With more efforts continuously

devoted by the global research community, new exciting progress is expected to occur in the following few years.

Acknowledgments
The authors would like to thank the Australian Research Council for supporting the project under contracts DP150104365 and DP160104835.

References

[1] B. Dunn, H. Kamath, J.-M. Tarascon, Science 334 (2011) 928–935.
[2] G. Xu, P. Nie, H. Dou, B. Ding, L. Li, X. Zhang, Mater. Today 20 (2017) 191–209.
[3] D. Lin, Y. Liu, Y. Cui, Nat. Nanotechnol. 12 (2017) 194–206.
[4] N. Nitta, F. Wu, J.T. Lee, G. Yushin, Mater. Today 18 (2015) 252–264.
[5] R. Chen, W. Qu, X. Guo, L. Li, F. Wu, Mater. Horiz. 3 (2016) 487–516.
[6] F. Wu, G. Yushin, Energy Environ. Sci. 10 (2017) 435–459.
[7] V. Aravindan, J. Gnanaraj, Y.-S. Lee, S. Madhavi, Chem. Rev. 114 (2014) 11619–11635.
[8] S.-H. Yu, X. Feng, N. Zhang, J. Seok, H.D. Abruña, Acc. Chem. Res. 51 (2018) 273–281.
[9] S.-H. Yu, S.H. Lee, D.J. Lee, Y.-E. Sung, T. Hyeon, Small 12 (2016) 2146–2172.
[10] P.G. Bruce, S.A. Freunberger, L.J. Hardwick, J.-M. Tarascon, Nat. Mater. 11 (2012) 19–29.
[11] J. Park, S.-H. Yu, Y.-E. Sung, Nano Today 18 (2018) 35–64.
[12] D.A. Boyd, Angew. Chem. Int. Ed. 55 (2016) 15486–15502.
[13] A. Manthiram, Y. Fu, S.-H. Chung, C. Zu, Y.-S. Su, Chem. Rev. 114 (2014) 11751–11787.
[14] Z.W. Seh, Y. Sun, Q. Zhang, Y. Cui, Chem. Soc. Rev. 45 (2016) 5605–5634.
[15] Y.-S. Su, Y. Fu, T. Cochell, A. Manthiram, Nat. Commun. 4 (2013) 2985.
[16] X. Zhang, H. Xie, C.-S. Kim, K. Zaghib, A. Mauger, C.M. Julien, Mater. Sci. Eng., R 121 (2017) 1–29.
[17] Z. Zeng, X. Liu, Adv. Mater. Interfaces 5 (2018) 1701274.
[18] L. Ma, K.E. Hendrickson, S. Wei, L.A. Archer, Nano Today 10 (2015) 315–338.
[19] G. Li, S. Wang, Y. Zhang, M. Li, Z. Chen, J. Lu, Adv. Mater. 30 (2018) 1705590.
[20] S. Xin, L. Gu, N.-H. Zhao, Y.-X. Yin, L.-J. Zhou, Y.-G. Guo, L.-J. Wan J. Am. Chem. Soc. 134 (2012) 18510–18513.
[21] Y.-X. Yin, S. Xin, Y.-G. Guo, L.-J. Wan, Angew. Chem. Int. Ed. 52 (2013) 13186–13200.
[22] M. Liu, F. Ye, W. Li, H. Li, Y. Zhang, Nano Res. 9 (2016) 94–116.
[23] T. Tao, S. Lu, Y. Fan, W. Lei, S. Huang, Y. Chen, Adv. Mater. 29 (2017) 1700542.
[24] L.F. Nazar, M. Cuisinier, Q. Pang, MRS Bull. 39 (2014) 436–442.
[25] R. Fang, S. Zhao, Z. Sun, D.-W. Wang, H.-M. Cheng, F. Li, Adv. Mater. 29 (2017) 1606823.
[26] R. Xu, J. Lu, K. Amine, Adv. Energy Mater. 5 (2015) 1500408.
[27] B. Zhang, X. Qin, G.R. Li, X.P. Gao, Energy Environ. Sci. 3 (2010) 1531–1537.
[28] X. Ji, K.T. Lee, L.F. Nazar, Nat. Mater. 8 (2009) 500–506.
[29] G. He, S. Evers, X. Liang, M. Cuisinier, A. Garsuch, L.F. Nazar, ACS Nano 7 (2013) 10920–10930.
[30] Y. Zhong, Q. Lu, Y. Zhu, Y. Zhu, W. Zhou, S. Wang, Z. Shao, Adv. Sustainable Syst. 1 (2017) 1700081.

[31] Q. Lu, Y. Zhong, W. Zhou, K. Liao, Z. Shao, Adv. Mater. Interfaces 5 (2018) 1701659.
[32] M.-Q. Zhao, Q. Zhang, J.-Q. Huang, G.-L. Tian, J.-Q. Nie, H.-J. Peng, F. Wei, Nat. Commun. 5 (2014) 3410.
[33] G. Zhou, S. Pei, L. Li, D.-W. Wang, S. Wang, K. Huang, L.-C. Yin, F. Li, H.-M. Cheng, Adv. Mater. 26 (2014) 625–631.
[34] J. Xu, J. Shui, J. Wang, M. Wang, H.-K. Liu, S.X. Dou, I.-Y. Jeon, J.-M. Seo, J.-B. Baek, L. Dai, ACS Nano 8 (2014) 10920–10930.
[35] W. Liu, J. Jiang, K.R. Yang, Y. Mi, P. Kumaravadivel, Y. Zhong, Q. Fan, Z. Weng, Z. Wu, J.J. Cha, H. Zhou, V.S. Batista, G.W. Brudvig, H. Wang, Proc. Natl. Acad. Sci. U.S.A. 114 (2017) 3578–3583.
[36] L. Ji, M. Rao, H. Zheng, L. Zhang, Y. Li, W. Duan, J. Guo, E.J. Cairns, Y. Zhang, J. Am. Chem. Soc. 133 (2011) 18522–18525.
[37] J. Guo, Y. Xu, C. Wang, Nano Lett. 11 (2011) 4288–4294.
[38] Y.C. Jeong, K. Lee, T. Kim, J.H. Kim, J. Park, Y.S. Cho, S.J. Yang, C.R. Park, J. Mater. Chem. A 4 (2016) 819–826.
[39] F. Jin, S. Xiao, L. Lu, Y. Wang, Nano Lett. 16 (2016) 440–447.
[40] Z.W. Seh, W. Li, J.J. Cha, G. Zheng, Y. Yang, M.T. McDowell, P.-C. Hsu, Y. Cui, Nat. Commun. 4 (2013) 1331.
[41] X. Liang, C. Hart, Q. Pang, A. Garsuch, T. Weiss, L.F. Nazar, Nat. Commun. 6 (2015) 5682.
[42] Z. Hao, R. Zeng, L. Yuan, Q. Bing, J. Liu, J. Xiang, Y. Huang, Nano Energy 40 (2017) 360–368.
[43] Z. Yuan, H.-J. Peng, T.-Z. Hou, J.-Q. Huang, C.-M. Chen, D.-W. Wang, X.-B. Cheng, F. Wei, Q. Zhang, Nano Lett. 16 (2016) 519–527.
[44] Q. Pang, D. Kundu, L.F. Nazar, Mater. Horiz. 3 (2016) 130–136.
[45] Z. Sun, J. Zhang, L. Yin, G. Hu, R. Fang, H.-M. Cheng, F. Li, Nat. Commun. 8 (2017) 14627.
[46] Q. Pang, X. Liang, C.Y. Kwok, L.F. Nazar, Nat. Energy 1 (2016) 16132.
[47] H. Furukawa, K.E. Cordova, M. O'Keeffe, O.M. Yaghi, Science 341 (2013) 1230444.
[48] L. Song, J. Zhang, L. Sun, F. Xu, F. Li, H. Zhang, X. Si, C. Jiao, Z. Li, S. Liu, Y. Liu, H. Zhou, D. Sun, Y. Du, Z. Cao, Z. Gabelica, Energy Environ. Sci. 5 (2012) 7508–7520.
[49] H. Wang, Q.-L. Zhu, R. Zou, Q. Xu, Chem 2 (2017) 52–80.
[50] F.-Y. Yi, R. Zhang, H. Wang, L.-F. Chen, L. Han, H.-L. Jiang, Q. Xu, Small Methods 1 (2017) 1700187.
[51] W. Wang, X. Xu, W. Zhou, Z. Shao, Adv. Sci. 4 (2017) 1600371.
[52] R. Demir-Cakan, M. Morcrette, F. Nouar, C. Davoisne, T. Devic, D. Gonbeau, R. Dominko, C. Serre, G. Férey, J.-M. Tarascon, J. Am. Chem. Soc. 133 (2011) 16154–16160.
[53] J. Zhou, R. Li, X. Fan, Y. Chen, R. Han, W. Li, J. Zheng, B. Wang, X. Li, Energy Environ. Sci. 7 (2014) 2715–2724.
[54] J. Zhou, X. Yu, X. Fan, X. Wang, H. Li, Y. Zhang, W. Li, J. Zheng, B. Wang, X. Li, J. Mater. Chem. A 3 (2015) 8272–8275.
[55] Z. Wang, X. Li, Y. Cui, Y. Yang, H. Pan, Z. Wang, C. Wu, B. Chen, G. Qian, Cryst. Growth Des. 13 (2013) 5116–5120.
[56] Y. Mao, G. Li, Y. Guo, Z. Li, C. Liang, X. Peng, Z. Lin, Nat. Commun. 8 (2017) 14628.
[57] Z. Zhao, S. Wang, R. Liang, Z. Li, Z. Shi, G. Chen, J. Mater. Chem. A 2 (2014) 13509–13512.

[58] P.M. Shanthi, P.J. Hanumantha, B. Gattu, M. Sweeney, M.K. Datta, P.N. Kumta, Electrochim. Acta 229 (2017) 208–218.
[59] Y.-S. Su, A. Manthiram, Nat. Commun. 3 (2012) 1166.
[60] Y.-S. Su, A. Manthiram, Chem. Commun. 48 (2012) 8817–8819.
[61] S. Bai, X. Liu, K. Zhu, S. Wu, H. Zhou, Nat. Energy 1 (2016) 16094.
[62] Q. Pang, X. Liang, C.Y. Kwok, L.F. Nazar, J. Electrochem. Soc. 162 (2015) A2567–A2576.
[63] W. Xia, A. Mahmood, R. Zou, Q. Xu, Energy Environ. Sci. 8 (2015) 1837–1866.
[64] X. Cao, C. Tan, M. Sindoro, H. Zhang, Chem. Soc. Rev. 46 (2017) 2660–2677.
[65] J. Xu, T. Lawson, H. Fan, D. Su, G. Wang, Adv. Energy Mater. 8 (2018) 1702607.
[66] F.-S. Ke, Y.-S. Wu, H. Deng, J. Solid State Chem. 223 (2015) 109–121.
[67] Z. Hu, D. Zhao, CrystEngComm 19 (2017) 4066–4081.
[68] Z. Wang, Z. Dou, Y. Cui, Y. Yang, Z. Wang, G. Qian, Microporous Mesoporous Mater. 185 (2014) 92–96.
[69] W. Bao, Z. Zhang, Y. Qu, C. Zhou, X. Wang, J. Li, J. Alloys Compd. 582 (2014) 334–340.
[70] Y. Yue, B. Guo, Z.-A. Qiao, P.F. Fulvio, J. Chen, A.J. Binder, C. Tian, S. Dai, Microporous Mesoporous Mater. 198 (2014) 139–143.
[71] L. Bai, D. Chao, P. Xing, L.J. Tou, Z. Chen, A. Jana, Z.X. Shen, Y. Zhao, ACS Appl. Mat. Interfaces 8 (2016) 14328–14333.
[72] Y. Feng, Y. Zhang, G. Du, J. Zhang, X. Qu, Sustainable Energy Fuels 2 (2018) 1828–1836.
[73] X. Ge, C. Li, Z. Li, L. Yin, Electrochim. Acta 281 (2018) 700–709.
[74] Y. Hou, H. Mao, L. Xu, Nano Res. 10 (2017) 344–353.
[75] W.-W. Jin, H.-J. Li, J.-Z. Zou, S.-Z. Zeng, Q.-D. Li, G.-Z. Xu, H.-C. Sheng, B.-B. Wang, Y.-H. Si, L. Yu, X.-R. Zeng, RSC Adv. 8 (2018) 4786–4793.
[76] H. Jiang, X.-C. Liu, Y. Wu, Y. Shu, X. Gong, F.-S. Ke, H. Deng, Angew. Chem. Int. Ed. 57 (2018) 3916–3921.
[77] A.E. Baumann, G.E. Aversa, A. Roy, M.L. Falk, N.M. Bedford, V.S. Thoi, J. Mater. Chem. A 6 (2018) 4811–4821.
[78] H. Zhang, W. Zhao, M. Zou, Y. Wang, Y. Chen, L. Xu, H. Wu, A. Cao, Adv. Energy Mater. 8 (2018) 1800013.
[79] J. Zheng, J. Tian, D. Wu, M. Gu, W. Xu, C. Wang, F. Gao, M.H. Engelhard, J.-G. Zhang, J. Liu, J. Xiao, Nano Lett. 14 (2014) 2345–2352.
[80] Z. Wang, B. Wang, Y. Yang, Y. Cui, Z. Wang, B. Chen, G. Qian, ACS Appl. Mat. Interfaces 7 (2015) 20999–21004.
[81] M.-T. Li, Y. Sun, K.-S. Zhao, Z. Wang, X.-L. Wang, Z.-M. Su, H.-M. Xie, ACS Appl. Mat. Interfaces 8 (2016) 33183–33188.
[82] J.H. Park, K.M. Choi, D.K. Lee, B.C. Moon, S.R. Shin, M.-K. Song, J.K. Kang, Sci. Rep. 6 (2016) 25555.
[83] Y. Pu, W. Wu, J. Liu, T. Liu, F. Ding, J. Zhang, Z. Tang, RSC Adv. 8 (2018) 18604–18612.
[84] D. Su, M. Cortie, H. Fan, G. Wang, Adv. Mater. 29 (2017) 1700587.
[85] X.-J. Hong, T.-X. Tan, Y.-K. Guo, X.-Y. Tang, J.-Y. Wang, W. Qin, Y.-P. Cai, Nanoscale 10 (2018) 2774–2780.
[86] H. Park, D.J. Siegel, Chem. Mater. 29 (2017) 4932–4939.
[87] H. Irving, R. Williams, J. Chem. Soc. (1953) 3192–3210.
[88] L. Sun, M.G. Campbell, M. Dincă, Angew. Chem. Int. Ed., 55 (2016) 3566–3579.
[89] F. Li, X. Zhang, X. Liu, M. Zhao, ACS Appl. Mat. Interfaces 10 (2018) 15012–15020.
[90] H.B. Wu, S. Wei, L. Zhang, R. Xu, H.H. Hng, X.W. Lou, Chem. Eur. J. 19 (2013) 10804–10808.

[91] Y. Zhu, G. Chen, X. Xu, G. Yang, M. Liu, Z. Shao, ACS Catal. 7 (2017) 3540–3547.
[92] Y. Liu, Z. Wang, Y. Zhong, M. Tade, W. Zhou, Z. Shao, Adv. Funct. Mater. 27 (2017) 1701229.
[93] Y. Zhong, S. Wang, Y. Sha, M. Liu, R. Cai, L. Li, Z. Shao, J. Mater. Chem. A 4 (2016) 9526–9535.
[94] R. Chen, T. Zhao, T. Tian, S. Cao, P.R. Coxon, K. Xi, D. Fairen-Jimenez, R.V. Kumar, A.K. Cheetham, APL Mater. 2 (2014) 124109.
[95] Z. Li, L. Yin, ACS Appl. Mat. Interfaces 7 (2015) 4029–4038.
[96] B. Ding, J. Wang, Z. Chang, G. Xu, X. Hao, L. Shen, H. Dou, X. Zhang, ChemElectroChem 3 (2016) 668–674.
[97] X. Li, Q. Sun, J. Liu, B. Xiao, R. Li, X. Sun, J. Power Sources 302 (2016) 174–179.
[98] Y. Jiang, H. Liu, X. Tan, L. Guo, J. Zhang, S. Liu, Y. Guo, J. Zhang, H. Wang, W. Chu, ACS Appl. Mater. Interfaces 9 (2017) 25239–25249.
[99] Y. Tan, Z. Jia, P. Lou, Z. Cui, X. Guo, J. Power Sources 341 (2017) 68–74.
[100] M. Yang, X. Hu, Z. Fang, L. Sun, Z. Yuan, S. Wang, W. Hong, X. Chen, D. Yu, Adv. Funct. Mater. 27 (2017) 1701971.
[101] R.-S. Song, B. Wang, T.-T. Ruan, L. Wang, H. Luo, F. Wang, T.-T. Gao, D.-L. Wang, Appl. Surf. Sci. 427 (2018) 396–404.
[102] J. Zhang, M. Huang, B. Xi, K. Mi, A. Yuan, S. Xiong, Adv. Energy Mater. 8 (2018) 1701330.
[103] Y. Tan, Z. Zheng, S. Huang, Y. Wang, Z. Cui, J. Liu, X. Guo, J. Mater. Chem. A 5 (2017) 8360–8366.
[104] Z. Chang, B. Ding, H. Dou, J. Wang, G Xu, X. Zhang, Chem. Eur. J. 24 (2018) 3768–3775.
[105] K. Chen, Z. Sun, R. Fang, Y. Shi, H.-M. Cheng, F. Li, Adv. Funct. Mater. (2018) 1707592, in press. DOI: 10.1002/adfm.201707592.
[106] G. Xu, B. Ding, L. Shen, P. Nie, J. Han, X. Zhang, J. Mater. Chem. A 1 (2013) 4490–4496.
[107] W. Bao, Z. Zhang, W. Chen, C. Zhou, Y. Lai, J. Li, Electrochim. Acta 127 (2014) 342–348.
[108] W. Bao, Z. Zhang, C. Zhou, Y. Lai, J. Li, J. of Power Sources, 248 (2014) 570–576.
[109] S. Cai, X. Wang, M. Chen, J. Liu, Q. Lu, S. Wei, J. Electrochem. Soc. 163 (2016) A2922–A2929.
[110] K. Xi, S. Cao, X. Peng, C. Ducati, R.V. Kumar, A.K. Cheetham, Chem. Commun. 49 (2013) 2192–2194.
[111] M. Klose, K. Pinkert, M. Zier, M. Uhlemann, F. Wolke, T. Jaumann, P. Jehnichen, D. Wadewitz, S. Oswald, J. Eckert, L. Giebeler, Carbon 79 (2014) 302–309.
[112] X. Qian, L. Jin, S. Wang, S. Yao, D. Rao, X. Shen, X. Xi, J. Xiang, RSC Adv. 6 (2016) 94629–94635.
[113] X.-J. Hong, X.-Y. Tang, Q. Wei, C.-L. Song, S.-Y. Wang, R.-F. Dong, Y.-P. Cai, L.-P. Si, ACS Appl. Mat. Interfaces 10 (2018) 9435–9443.
[114] X. Wang, X. Fang, X. Guo, Z. Wang, L. Chen, Electrochim. Acta 97 (2013) 238–243.
[115] X. Meng, Q. Gao, Chem. J. Chin. Univ.-Chin. 35 (2014) 1715–1719.
[116] X. Yang, N. Yan, W. Zhou, H. Zhang, X. Li, H. Zhang, J. Mater. Chem. A 3 (2015) 15314–15323.
[117] X. Yang, Y. Yu, N. Yan, H. Zhang, X. Li, H. Zhang, J. Mater. Chem. A 4 (2016) 5965–5972.
[118] G.-P. Hao, C. Tang, E. Zhang, P. Zhai, J. Yin, W. Zhu, Q. Zhang, S. Kaskel, Adv. Mater. 29 (2017) 1702829.
[119] Y. Liu, G. Li, J. Fu, Z. Chen, X. Peng, Angew. Chem. Int. Ed. 56 (2017) 6176–6180.

[120] H. Zhang, Z. Zhao, Y. Liu, J. Liang, Y. Hou, Z. Zhang, X. Wang, J. Qiu, J. Energy Chem. 26 (2017) 1282–1290.
[121] Y.-J. Li, J.-M. Fan, M.-S. Zheng, Q.-F. Dong, Energy Environ. Sci. 9 (2016) 1998–2004.
[122] J. He, Y. Chen, W. Lv, K. Wen, C. Xu, W. Zhang, Y. Li, W. Qin, W. He, ACS Nano 10 (2016) 10981–10987.
[123] Z. Li, C. Li, X. Ge, J. Ma, Z. Zhang, Q. Li, C. Wang, L. Yin, Nano Energy 23 (2016) 15–26.
[124] Y. Li, J. Fang, J. Zhang, J. Yang, R. Yuan, J. Chang, M. Zheng, Q. Dong, ACS Nano 11 (2017) 11417–11424.
[125] D. Xiao, Q. Li, H. Zhang, Y. Ma, C. Lu, C. Chen, Y. Liu, S. Yuan, J. Mater. Chem. A 5 (2017) 24901–24908.
[126] S. Luo, C. Zheng, Y. Li, S. Liu, Journal of Power and Energy Engineering 5 (2017) 16–20.
[127] J.Y. Hong, Y. Jung, D.-W. Park, S. Chung, S. Kim, Electrochim. Acta 259 (2018) 1021–1029.
[128] J. Zhao, C. Liu, H. Deng, S. Tang, C. Liu, S. Chen, J. Guo, Q. Lan, Y. Li, Y. Liu, M. Ye, H. Liu, J. Liang, Y.-C. Cao, Mater. Today Energy 8 (2018) 134–142.
[129] H. Lu, C. Zhang, Y. Zhang, Y. Huang, M. Liu, T. Liu, Nano Res. (2018) in press. DOI: 10.1007/s12274-018-2130-9.
[130] G. Li, W. Lei, D. Luo, Y. Deng, Z. Deng, D. Wang, A. Yu, Z. Chen, Energy Environ. Sci. (2018) in press. DOI: 10.1039/c8ee01377b.
[131] J. Xu, W. Zhang, Y. Chen, H. Fan, D. Su, G. Wang, J. Mater. Chem. A 6 (2018) 2797–2807.
[132] J. Zhou, N. Lin, W.L. Cai, C. Guo, K. Zhang, J. Zhou, Y. Zhu, Y. Qian, Electrochim. Acta 218 (2016) 243–251.
[133] T. Chen, Z. Zhang, B. Cheng, R. Chen, Y. Hu, L. Ma, G. Zhu, J. Liu, Z. Jin, J. Am. Chem. Soc. 139 (2017) 12710–12715.
[134] J. He, Y. Chen, A. Manthiram, iScience 4 (2018) 36–43.
[135] C. Li, Z. Xi, S. Dong, X. Ge, Z. Li, C. Wang, L. Yin, Energy Storage Mater. 12 (2018) 341–351.
[136] W. Bao, D. Su, W. Zhang, X. Guo, G. Wang, Adv. Funct. Mater. 26 (2016) 8746–8756.
[137] T. Dhawa, S. Chattopadhy, G. De, S. Mahanty, ACS Omega 2 (2017) 6481–6491.
[138] Z. Li, R. Soc. Open Sci. 5 (2018) 171824.
[139] J. Cheng, D. Zhao, L. Fan, X. Wu, M. Wang, H. Wu, B. Guan, N. Zhang, K. Sun, Chem. Eur. J. (2018) in press. DOI: 10.1002/chem.201801939.
[140] S.S. Zhang, J. Power Sources 231 (2013) 153–162.
[141] J. Gao, H.D. Abruña, J. Phys. Chem. Lett. 5 (2014) 882–885.
[142] T.-Z. Hou, X. Chen, H.-J. Peng, J.-Q. Huang, B.-Q. Li, Q. Zhang, B. Li, Small 12 (2016) 3283–3291.
[143] J. Zhang, H. Hu, Z. Li, X.W. Lou, Angew. Chem. Int. Ed. 55 (2016) 3982–3986.
[144] C. Li, Z. Li, Q. Li, Z. Zhang, S. Dong, L. Yin, Electrochim. Acta 215 (2016) 689–698.
[145] H. Wei, E.F. Rodriguez, A.S. Best, A.F. Hollenkamp, D. Chen, R.A. Caruso, Adv. Energy Mater. 7 (2017) 1601616.
[146] S. Mei, C.J. Jafta, I. Lauermann, Q. Ran, M. Kärgell, M. Ballauff, Y. Lu, Adv. Funct. Mater. 27 (2017) 1701176.
[147] G. Zhou, H. Tian, Y. Jin, X. Tao, B. Liu, R. Zhang, Z.W. Seh, D. Zhuo, Y. Liu, J. Sun, J. Zhao, C. Zu, D.S. Wu, Q. Zhang, Y. Cui, Proc. Natl. Acad. Sci. U.S.A. 114 (2017) 840–845.
[148] X. Liang, A. Garsuch, L.F. Nazar, Angew. Chem. Int. Ed. 54 (2015) 3907–3911.

[149] H. Zhang, Z. Zhao, Y.-N. Hou, Y. Tang, Y. Dong, S. Wang, X. Hu, Z. Zhang, X. Wang, J. Qiu, J. Mater. Chem. A, 6 (2018) 7133–7141.
[150] Y. An, Z. Zhang, H. Fei, S. Xiong, B. Ji, J. Feng, ACS Appl. Mat. Interfaces 9 (2017) 12400–12407.
[151] J. Wang, T. Wu, S. Zhang, S. Gu, J. Jin, Z. Wen, Chem. Eng. J. 334 (2018) 2356–2362.
[152] D.H. Lee, J.H. Ahn, M.-S. Park, A. Eftekhari, D.-W. Kim, Electrochim. Acta 283 (2018) 1291–1299.
[153] F. Wu, S. Zhao, L. Chen, Y. Lu, Y. Su, Y. Jia, L. Bao, J. Wang, S. Chen, R. Chen, Energy Storage Mater. 14 (2018) 383–391.
[154] J.-K. Huang, M. Li, Y. Wan, S. Dey, M. Ostwal, D. Zhang, C.-W. Yang, C.-J. Su, U-S. Jeng, J. Ming, A. Amassian, Z. Lai, Y. Han, S. Li, L.-J. Li, ACS Nano 12 (2018) 836–843.
[155] J. He, Y. Chen, A. Manthiram, Energy Environ. Sci. (2018) in press. DOI: 10.1039/c8ee00893k.
[156] S. Bai, K. Zhu, S. Wu, Y. Wang, J. Yi, M. Ishida, H. Zhou, J. Mater. Chem. A 4 (2016) 16812–16817.
[157] P. Chiochan, S. Kaewruang, N. Phattharasupakun, J. Wutthiprom, T. Maihom, J. Limtrakul, S. Nagarkar, S. Horike, M. Sawangphruk, Sci. Rep. 7 (2017) 17703.
[158] M. Li, Y. Wan, J.-K. Huang, A.H. Assen, C.-E. Hsiung, H. Jiang, Y. Han, M. Eddaoudi, Z. Lai, J. Ming, L.-J. Li, ACS Energy Lett. 2 (2017) 2362–2367.
[159] S. Suriyakumar, M. Kanagaraj, M. Kathiresan, N. Angulakshmi, S. Thomas, A.M. Stephan, Electrochim. Acta 265 (2018) 151–159.
[160] S. Suriyakumar, A.M. Stephan, N. Angulakshmi, M.H. Hassan, M.H. Alkordi, J. Mater. Chem. A 6 (2018) 14623–14632.
[161] Y. Guo, M. Sun, H. Liang, W. Ying, X. Zeng, Y. Ying, S. Zhou, C. Liang, Z. Lin, X. Peng, ACS Appl. Mat. Interfaces (2018) in press. DOI: 10.1021/acsami.8b11042.
[162] Y. Zhou, C. Zhou, Q. Li, C. Yan, B. Han, K. Xia, Q. Gao, J. Wu, Adv. Mater. 27 (2015) 3774–3781.
[163] W. Qian, Q. Gao, Z. Li, W. Tian, H. Zhang, Q. Zhang, ACS Appl. Mat. Interfaces 9 (2017) 28366–28376.
[164] Y.-C. Lu, Q. He, H.A. Gasteiger, J. Phys. Chem. C 118 (2014) 5733–5741.
[165] Z. Wang, R. Tan, H. Wang, L. Yang, J. Hu, H. Chen, F. Pan, Adv. Mater. 30 (2018) 1704436.
[166] C. Serre, Nat. Energy 1 (2016) 16100.
[167] S. Wei, S. Xu, A. Agrawral, S. Choudhury, Y. Lu, Z. Tu, L. Ma, L.A. Archer, Nat. Commun. 7 (2016) 11722.
[168] Y.-M. Chen, W. Liang, S. Li, F. Zou, S.M. Bhaway, Z. Qiang, M. Gao, B.D. Vogt, Y. Zhu, J. Mater. Chem. A 4 (2016) 12471–12478.
[169] S.-K. Park, J.-S. Park, Y.C. Kang, J. Mater. Chem. A 6 (2018) 1028–1036.
[170] J. He, W. Lv, Y. Chen, J. Xiong, K. Wen, C. Xu, W. Zhang, Y. Li, W. Qin, W. He, J. Power Sources 363 (2017) 103–109.
[171] Z. Li, L. Yin, Nanoscale 7 (2015) 9597–9606.
[172] Q. Xu, T. Liu, Y. Li, L. Hu, C. Dai, Y. Zhang, Y. Li, D. Liu, M. Xu, ACS Appl. Mat. Interfaces 9 (2017) 41339–41346.